Article

Cell Reports

MyT1 Counteracts the Neural Progenitor Program to Promote Vertebrate Neurogenesis

Graphical Abstract

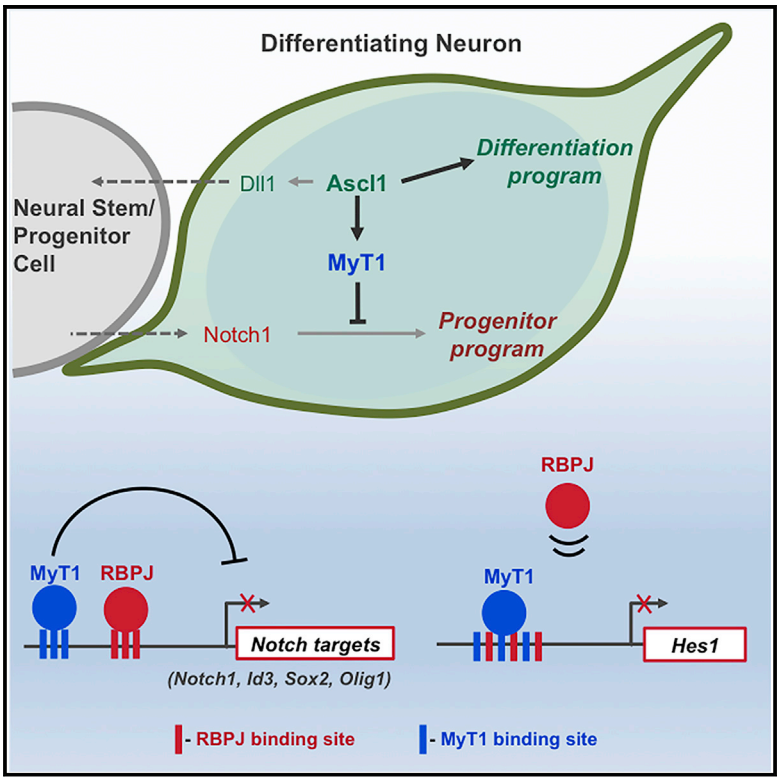

Authors

Francisca F. Vasconcelos, Alessandro Sessa, Cátia Laranjeira, ..., Jonas Muhr, Vania Broccoli, Diogo S. Castro

Correspondence

dscastro@igc.gulbenkian.pt

In Brief

Vasconcelos et al. find that the transcription factor MyT1 promotes neuronal differentiation downstream the proneural factor Ascl1. MyT1 represses the transcription of Notch signaling components and targets genes, including important regulators of the neural progenitor program. Thus, Ascl1 activates differentiation genes while repressing the progenitor program via MyT1.

Highlights

- MyT1 promotes neurogenesis downstream Ascl1
- MyT1 represses *Notch1* receptor and many of its downstream target genes
- MyT1 represses *Hes1* expression by direct DNA binding and competition with RBPJ
- Ascl1 suppresses Notch signaling cell-autonomously while promoting differentiation

Accession Numbers

E-MTAB-4330
E-MTAB-4494
E-MTAB-4335
E-MTAB-4331

Vasconcelos et al., 2016, Cell Reports *17*, 469–483
October 4, 2016
http://dx.doi.org/10.1016/j.celrep.2016.09.024

Cell Reports
Article

MyT1 Counteracts the Neural Progenitor Program to Promote Vertebrate Neurogenesis

Francisca F. Vasconcelos,[1] Alessandro Sessa,[2] Cátia Laranjeira,[1] Alexandre A.S.F. Raposo,[1] Vera Teixeira,[1] Daniel W. Hagey,[3] Diogo M. Tomaz,[1] Jonas Muhr,[3] Vania Broccoli,[2] and Diogo S. Castro[1,4,*]
[1]Instituto Gulbenkian de Ciência, 2780-156 Oeiras, Portugal
[2]Division of Neuroscience, San Raffaele Scientific Institute, 20132 Milan, Italy
[3]Department of Cell and Molecular Biology, Ludwig Institute for Cancer Research, Karolinska Institutet, 17177 Stockholm, Sweden
[4]Lead Contact
*Correspondence: dscastro@igc.gulbenkian.pt
http://dx.doi.org/10.1016/j.celrep.2016.09.024

SUMMARY

The generation of neurons from neural stem cells requires large-scale changes in gene expression that are controlled to a large extent by proneural transcription factors, such as Ascl1. While recent studies have characterized the differentiation genes activated by proneural factors, less is known on the mechanisms that suppress progenitor cell identity. Here, we show that Ascl1 induces the transcription factor MyT1 while promoting neuronal differentiation. We combined functional studies of MyT1 during neurogenesis with the characterization of its transcriptional program. MyT1 binding is associated with repression of gene transcription in neural progenitor cells. It promotes neuronal differentiation by counteracting the inhibitory activity of Notch signaling at multiple levels, targeting the Notch1 receptor and many of its downstream targets. These include regulators of the neural progenitor program, such as *Hes1*, *Sox2*, *Id3*, and *Olig1*. Thus, Ascl1 suppresses Notch signaling cell-autonomously via MyT1, coupling neuronal differentiation with repression of the progenitor fate.

INTRODUCTION

The generation of neurons in the developing vertebrate nervous system requires the progression through a succession of distinct cellular states. These transitions have been particularly well characterized in the embryonic telencephalon, where radial glia (RG) cells located in the ventricular zone (VZ) have characteristics of neural stem cells and constitute the major progenitor type during the neurogenic period (Götz and Huttner, 2005). Upon division, an RG cell can give rise to another RG cell and either a neuronal committed intermediate progenitor (IP) or a post-mitotic neuron that migrate toward the subventricular zone (SVZ) and cortical plate (CP), respectively (Kriegstein and Alvarez-Buylla, 2009). These events are known to be coordinated, to large extent, by the opposing activities of proneural and Notch pathways.

Proneural transcription factors, such as Ascl1 (also known as Mash1), are both required and sufficient to induce a complete program of neuronal differentiation (Bertrand et al., 2002; Vasconcelos and Castro, 2014; Wilkinson et al., 2013). While activating neuronal differentiation, proneural proteins induce the transcription of Notch ligands, such as *Dll1*. Dll1 interacts with a transmembrane Notch receptor in neighboring cells, resulting in cleavage of the Notch intracellular domain (NICD) by gamma-secretase and its nuclear translocation, forming a complex with the DNA-binding transcription factor Rbpj and additional coactivators. Direct targets of this complex include the transcriptional repressors Hes1 and Hes5, which repress the expression of proneural genes and neuronal differentiation via a process called lateral inhibition (Kageyama et al., 2008; Louvi and Artavanis-Tsakonas, 2006). The induction of differentiation by proneural factors requires, therefore, the simultaneous repression of Notch receptor activity in differentiating progenitors by mechanisms that remain poorly understood.

Myelin transcription factor 1 (MyT1 or NZF2) is the founding member of a family of zinc-finger proteins comprising also MyT1Like (MyT1L or NZF1) and MyT3 (NZF3 or St18) (Jiang et al., 1996; Kim and Hudson, 1992; Yee and Yu, 1998). All factors are expressed with distinct patterns throughout the mouse developing nervous system. In situ hybridization studies have described *Myt1* expression in differentiating progenitors and post-mitotic neuronal precursors, in both CNS and peripheral nervous system, starting at the beginning of the neurogenesis period (Matsushita et al., 2002, 2014). Evidence for a regulatory function of MyT1 in a neurogenic context was provided by functional studies in *Xenopus* embryos, where it counteracts lateral inhibition in synergy with the proneural factors X-Ngnr1, Xash3, or Xath5 (Bellefroid et al., 1996; Quan et al., 2004; Schneider et al., 2001). In mouse, the analysis of MyT1-null embryos has failed to provide insights into the function of MyT1 in the nervous system, presumably due to the observed ectopic upregulation of other family members in this mouse model (Hudson et al., 2011; Wang et al., 2007). More recently, the extensive use of MyT1L in neuronal reprogramming of mouse and human somatic cells (e.g., Pang et al., 2011 and Vierbuchen et al., 2010) has renewed the interest in understanding the function of MyT1 and its related factors in vertebrate neurogenesis.

Here, we identify MyT1 as a direct target of the proneural factor Ascl1 at the onset of neuronal differentiation, and we

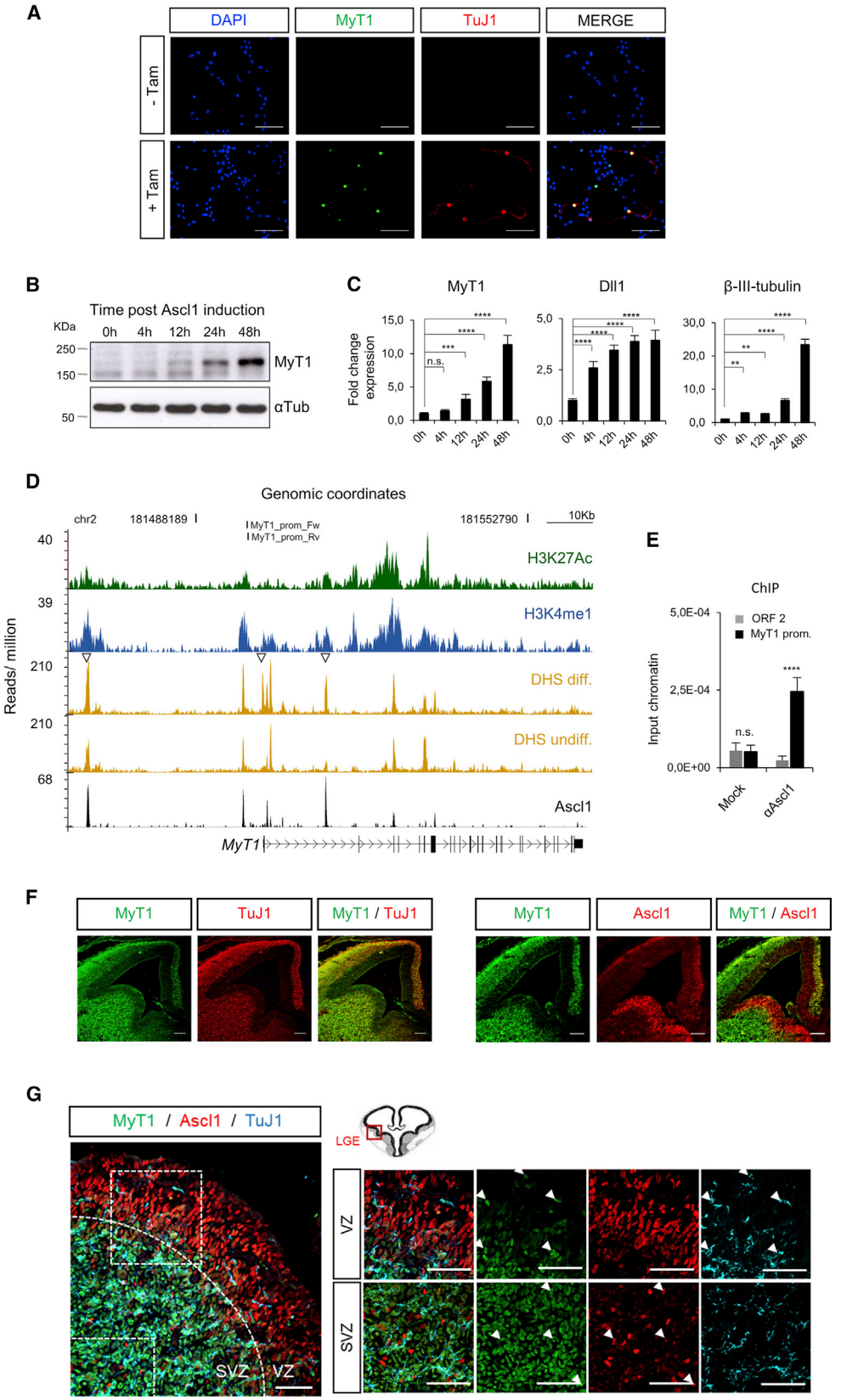

(legend on next page)

investigate the function of MyT1 at this critical stage by combining acute functional experiments in the mouse telencephalon with the characterization of its transcriptional program. We found that MyT1 binding occurs mostly at active regulatory regions in undifferentiated neural stem/progenitor cells and is associated with transcriptional repression genome-wide. We further show that MyT1 acts at multiple levels to antagonize the inhibitory activity of Notch signaling, targeting both Notch pathway components and downstream targets. Notably, MyT1 promotes the downregulation of *Hes1*, a determinant step for the onset of neurogenesis, by competing with Rbpj for binding to the *Hes1* promoter. Our results reveal a function of Ascl1 in inhibiting Notch signaling cell-autonomously, showing how activation of neuronal differentiation is tightly coordinated with repression of the progenitor program.

RESULTS

Ascl1 Directly Activates the Transcription Factor MyT1

Several observations have suggested the zinc-finger transcription factor MyT1 may be under the regulation of Ascl1. Specifically, *Myt1* expression is increased or decreased in expression profiling studies using DNA arrays upon Ascl1 gain and loss of function (GoF and LoF), respectively, both in mouse cultured neural stem/progenitor cells and in the embryonic telencephalon (Figure S1) (Castro et al., 2011; Gohlke et al., 2008; Raposo et al., 2015).

We started by analyzing the kinetics of MyT1 expression, using a cellular model of neurogenesis in which differentiation is triggered by the activation of an inducible version of Ascl1 protein (Ascl1-ERT2) in the neural stem cell line NS5 with 4-hydroxytamoxifen (Tam) (Raposo et al., 2015). Upon Ascl1 induction, MyT1 protein levels increased, as measured by immunocytochemistry and western blot (Figures 1A and 1B). Co-localization of MyT1 with the neuronal marker B-III-Tubulin (TuJ1) indicated that MyT1 expression occurred in differentiating neurons (Figure 1A). The increase in *Myt1* expression occurred after the increase in *Dll1* transcript, an early Ascl1 target gene, and preceded the increase in *B-III-Tubulin* transcript, an early neuronal marker that is also directly activated by Ascl1 (Castro et al., 2006, 2011) (Figure 1C). Thus, the timing of MyT1 induction is consistent with MyT1 being directly controlled by Ascl1.

Effectively, visual inspection of the chromatin immunoprecipitation followed by deep sequencing (ChIP-seq) enrichment profile of Ascl1-ERT2 in differentiating cells identified several peaks, corresponding to Ascl1 binding to active enhancer regions enriched for H3K4me1 and H3K27ac in the vicinity of the MyT1 gene (Figure 1D). Some Ascl1-binding events (BEs) occurred in closed chromatin regions in proliferating progenitors, which became opened during neuronal differentiation, as assessed by DNase sequencing (DNase-seq) (Figure 1D). This feature is associated with Ascl1 targets that are expressed de novo during differentiation (Raposo et al., 2015), and it may account for the late timing of MyT1 induction after Ascl1 expression. Ascl1 binding to *Myt1* promoter was further validated by ChIP-qPCR in chromatin extracted from the developing ventral telencephalon (Figure 1E).

MyT1 Promotes Neurogenesis in the Mouse Telencephalon

Myt1 transcript is expressed in the germinal layers during the neurogenic period in scattered cells in the VZ, with highest expression in the SVZ (Matsushita et al., 2002, 2014). In the ventral telencephalon, MyT1 protein expression domain largely overlapped with that of the neuronal marker TuJ1 (Figure 1F). At the cellular level, many, but not all, MyT1-expressing cells in the SVZ co-expressed TuJ1 (Figure 1G), suggesting MyT1 was expressed both in IPs and differentiating neurons. In addition, few MyT1-expressing cells were interspersed in the VZ co-expressing TuJ1 (Figure 1G, arrowheads in upper panels). Although MyT1 and Ascl1 expression domains were mostly non-overlapping (Figure 1F), some cells co-expressing both factors could be found in the SVZ (Figure 1G, arrowheads in bottom panels), as expected from Ascl1-expressing IPs. Overall, the expression pattern was consistent with MyT1 starting to be expressed at the transition from RG cells to differentiating neurons, either directly (VZ) or indirectly through the generation of IPs (SVZ). The persistent expression of MyT1 in post-mitotic neuronal precursors suggests a function also at later stages of neurogenesis.

We next investigated MyT1 function in the telencephalon by performing acute GoF and LoF experiments by in utero electroporation. We targeted the lateral ganglionic eminence (LGE) at embryonic day (E)12.5, a stage at which MyT1 is the only member of its family to be significantly expressed in germinal layers (Matsushita et al., 2002, 2014). MyT1 overexpression resulted

Figure 1. MyT1 Is a Direct Target of Ascl1 during Neuronal Differentiation

(A) Immunocytochemical analysis of MyT1 (green) and TuJ1 (red) before (−Tam) and 48 hr after Tam induction (+Tam). Cell nuclei are labeled with DAPI (blue). Scale bar, 50 μm.

(B) Analysis of MyT1 protein levels by western blot post-Tam induction. α-tubulin was used as a loading control.

(C) RNA expression analysis of *Myt1*, *Dll1*, and *B-III-Tubulin* by qPCR post-Tam induction is shown.

(D) Ascl1 (black), H3K27ac (green), and H3K4me1 (blue) ChIP-seq and DNase-seq enrichment profiles (yellow) at *Myt1* locus in undifferentiated and/or differentiating NS cells. MyT1 prom_Fw and MyT1 prom_Rv indicate genomic locations of primers used in (E).

(E) ChIP-qPCR of Ascl1 in chromatin extracted from E12.5 ventral telencephalon is shown. ORF1, negative control region; MyT1 prom., *Myt1* promoter region amplified using the primers highlighted in (D).

(F) Immunohistochemical analysis for MyT1 (green) and neuronal marker B-III-Tubulin (TuJ1, red) (left panel) or MyT1 (green) and Ascl1 (red) (right panel) in frontal sections of E14.5 mouse telencephalon is shown. Scale bar, 100 μm.

(G) Immunohistochemical analysis for MyT1 (green), Ascl1 (red), and TuJ1 (cyan) in frontal sections of E14.5 mouse ventral telencephalon. Dashed squares indicate magnified regions of VZ and SVZ. White arrowheads indicate co-localization of MyT1 and TuJ1 in the VZ (upper panel) or MyT1 and Ascl1 in the SVZ (lower panel). VZ, ventricular zone; SVZ, subventricular zone. Scale bar, 100 μm.

Data are shown as mean ± SD; n.s., $p > 0.05$; **$p < 0.01$, ***$p < 0.001$, and ****$p < 0.0001$, according to one-way ANOVA with Bonferroni correction for multiple testing (C) and Student's t test (E). See also Figure S1.

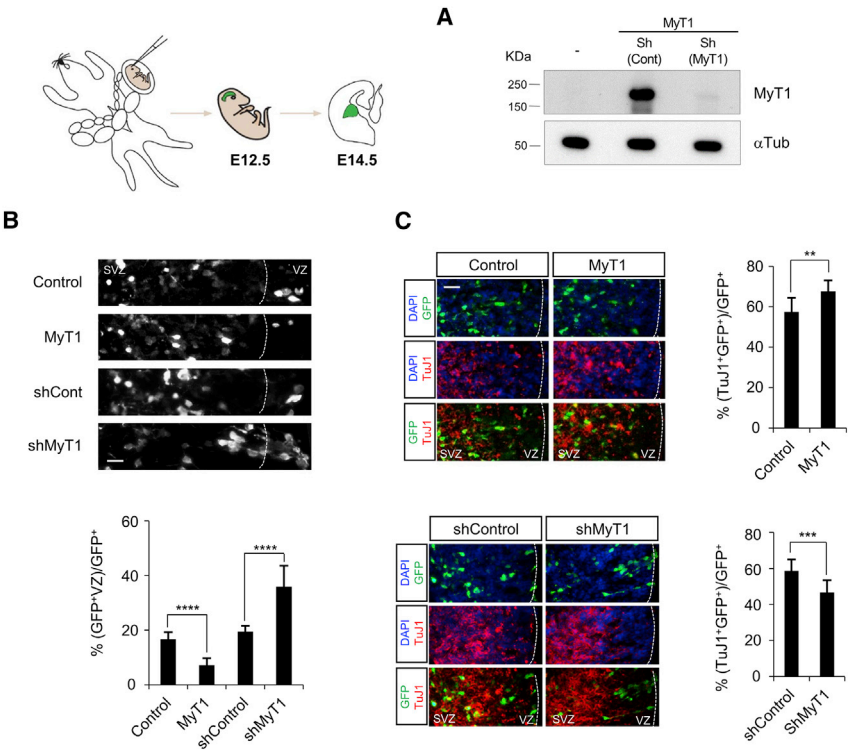

Figure 2. MyT1 Promotes Neurogenesis in the Developing Telencephalon

(A) Analysis by western blot of MyT1 in P19 cells co-transfected with MyT1 expression vector, scramble shRNA (shControl), and/or MyT1 shRNA (shMyT1). α-tubulin was used as a loading control.

(B and C) In utero electroporation of control or MyT1-, control shRNA- (shControl), or MyT1 shRNA- (shMyT1) expressing vectors in E12.5 mouse ventral telencephalon. Immunofluorescence analysis on a coronal section of the telencephalon for GFP (green or gray) and TuJ1 (red) 2 days post-electroporation (E14.5) is shown. Cell nuclei are labeled with DAPI (blue). Histograms represent the quantification of VZ to SVZ transition based on the fraction of GFP^+ cells that are retained in the VZ (GFP^+VZ/GFP^+) (B) and of neuronal differentiation based on the fraction of GFP^+ cells that express TuJ1 (($TuJ1^+GFP^+$)/GFP^+) (C). VZ, ventricular zone; SVZ, subventricular zone. Scale bars, 20 and 50 μm (B and C).

Data are shown as mean ± SD; **p < 0.01, ***p < 0.001, and ****p < 0.0001, according to Student's t test (B and C). See also Figure S2.

in more cells (~56% increase) leaving the VZ, and this was associated with an increase in TuJ1-expressing cells (~20% more) when compared to control conditions (Figures 2B and 2C). By contrast, knockdown of MyT1 with a small hairpin RNA (shRNA) expression vector (ShMyT1) (Figure 2A) resulted in more cells remaining in the VZ (~85% increase) and fewer TuJ1-positive cells (~17.4% decrease) (Figures 2B and 2C). We analyzed if the concomitant induction of other family members could be compensating the extent of the phenotype observed, by knocking down MyT1 together with MyT1L or MyT3. Indeed, a significant enhancement of the phenotype was observed when combining shMyT1 with shMyT1L, both in number of cells retained in the VZ and in the number of TuJ1-positive cells (Figure S2); the combination with ShMyT3 did not increase significantly the phenotype triggered by shMyT1 alone. Altogether, these experiments demonstrate that MyT1 promotes neurogenesis in the developing mouse embryo.

MyT1 Functions as a Transcriptional Repressor during Neurogenesis

To understand the molecular basis of MyT1 function at the onset of differentiation, we characterized its target genes upon acute GoF in neural stem/progenitor cells. For this, we infected NS5 cells with a lentivirus expressing a doxycycline (Dox)-inducible HA-tagged version of MyT1, and we characterized the gene expression changes 4 hr post MyT1 induction using DNA arrays (Figure S3). This identified 1,764 deregulated genes ($p < 0.05$), of which 57% were downregulated and 43% were upregulated (Table S1). We performed genome-wide mapping of MyT1 binding by ChIP-seq using an antibody against the HA-tag of MyT1, and we identified 7,615 BEs ($q < 10^{-2}$) associated with 4,448 unique genes following a nearest gene annotation (Table S2). A de novo search found the MyT1-binding motif (Gamsjaeger et al., 2008; Kim and Hudson, 1992) to be enriched at peak summits, with peaks with one or multiple motifs significantly enriched when compared to a control dataset (Figures 3A–3C). In addition, a compound Rfx/Rbpj motif, E box (bHLH) and Sox DNA-binding motifs were also overrepresented. Hierarchical clustering of MyT1 peaks according to the presence of these motifs revealed their occurrence was largely mutually exclusive (Figure S4A). Although the largest group bore the MyT1 motif, the data suggest that many MyT1 peaks result from indirect recruitment of MyT1 by other TFs.

Previous reports have implicated MyT1 both in transcriptional activation and repression (Bellefroid et al., 1996; Hu et al., 2013; Romm et al., 2005; Wang et al., 2008; Yokoyama et al., 2014). To gain an insight into the global transcriptional response mediated by MyT1, we integrated the location analysis of MyT1 with the expression profiling to find that 14% of sites are associated with a deregulated gene. Strikingly, MyT1 BEs were statistically significantly associated with downregulated genes ($p < 3.45 \times 10^{-51}$), whereas such association with upregulated genes was not found (Figure 3D). Notably, this differential association with downregulated genes was maintained when considering only peaks containing the MyT1 motif, or those without it (Figure S4B), suggesting that all types of MyT1 BEs are associated with repression of gene expression.

We next determined the fractions of up- and downregulated genes associated with at least one MyT1 BE (direct targets), considering increasing p value cutoffs for MyT1 binding (Figure 3E). We found that downregulated genes were strongly enriched for MyT1 direct targets, in contrast to upregulated genes (Figure 3E, compare Down/MyT1 with Up/MyT1), and that such

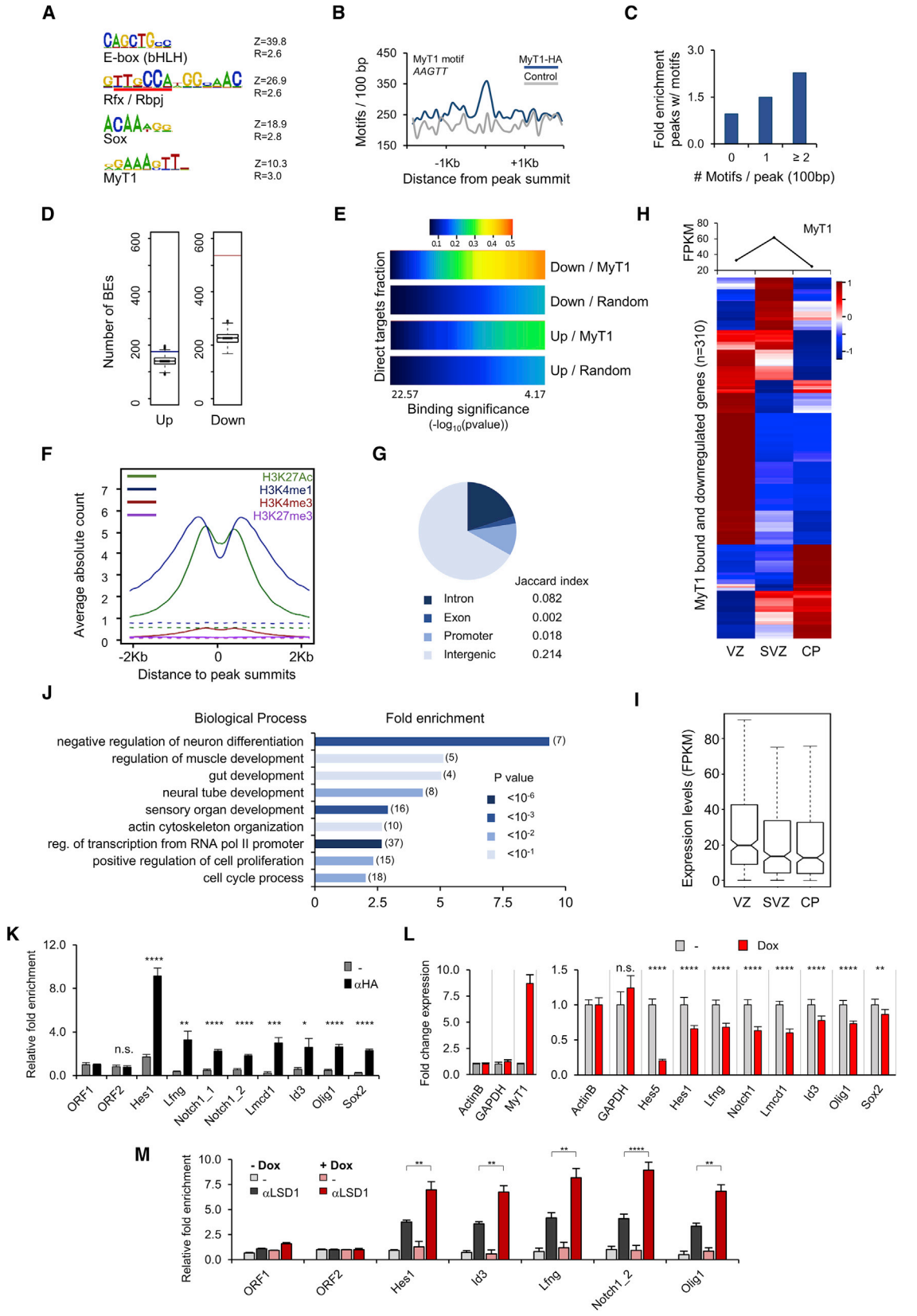

(legend on next page)

enrichment was statistically significant (Figure 3E, compare Down/MyT1 with Down/Random), confirming that MyT1 binding is associated with gene repression genome-wide.

Genome-wide maps of histone modifications in proliferating NS5 cells (Mikkelsen et al., 2007; Raposo et al., 2015) showed significant enrichment of H3K27ac, H3K4me1, and H3K4me3 at MyT1 BEs, as compared to random genomic regions (while no enrichment of the repressive mark H3K27me3 was found) (Figure 3F). In addition, most MyT1 BEs were found within intergenic or intronic regions, with a smaller but significant fraction occurring at gene promoters (Figure 3G). These results suggest that MyT1 binds to distal enhancer and promoter regions bearing active marks in neural stem/progenitor cells, and they are in line with MyT1's role as a transcriptional repressor at onset of differentiation.

MyT1 Represses Notch Pathway Components and Regulators of the Neural Progenitor Program

We next assessed the expression of the identified MyT1 targets (bound and downregulated) at distinct stages of the neuronal lineage, using expression profiling datasets representative of various layers of the E14.5 mouse embryonic cortex (Fietz et al., 2012). Notably, most MyT1 direct targets (69.0%) were downregulated during neuronal differentiation in vivo, as indicated by a decrease in expression from VZ to SVZ or CP (Figure 3H). In addition, their absolute levels of expression were highest at VZ, when compared to SVZ and CP (Figure 3I).

To investigate the function of MyT1 direct targets, we performed gene ontology (GO) analysis on a high-confidence list of 402 MyT1 targets (bound and repressed by MyT1) (Table S3). Enriched terms (GO biological processes) suggested a role in maintenance of a progenitor state (negative regulation of neuron differentiation, positive regulation of cell proliferation, and cell-cycle process), and they were associated with Notch pathway genes (e.g., *Notch1*, *Lfng*, *Dtx4*, and *Hes1*) (Figure 3J; Table S4). In addition, MyT1 targets encoded important transcriptional regulators (regulation of transcription from RNA polymerase II [Pol II] promoter) (Figure 3J) of the neural progenitor program, such as *Sox2*, *Id3*, and *Olig1* (Bai et al., 2007; Englund et al., 2005; Gómez-López et al., 2011) (Figures 3K and 3L; Table S4).

MyT1 has been shown to physically interact with the histone demethylase LSD1 in a complex that contains CoREST and promotes transcriptional repression (Yokoyama et al., 2014). To address if LSD1 is recruited by MyT1 to the abovementioned targets associated with a MyT1 motif, we performed anti-LSD1 ChIP-qPCR. We observed a substantial increase of LSD1 recruitment to MyT1 target sites upon MyT1 GoF, supporting a role for this histone demethylase in MyT1-mediated transcriptional repression in neural progenitor cells (Figure 3M).

MyT1 Promotes Neurogenesis by Counteracting Notch-Signaling Activity

Given the prominence of Notch-related genes among MyT1 targets and in line with previous findings (Bellefroid et al., 1996; Hu et al., 2013; Romm et al., 2005; Wang et al., 2008; Yokoyama et al., 2014), we tested if MyT1 can counteract the inhibitory effect of Notch signaling in neurogenesis. We infected NS5 cells with lentiviruses expressing Ascl1, MyT1, and a membrane-bound dominant active version of the Notch1 receptor, whose cleavage is independent of a ligand/receptor interaction (Act Notch). As expected, Ascl1 expression induced the generation of TuJ1-positive neurons with a concomitant decrease of Sox2 expression (Berninger et al., 2007; Farah et al., 2000; Nakada et al., 2004), and this effect was inhibited by the co-expression of Act Notch (Gaiano et al., 2000) (Figure 4A). Importantly, MyT1 alone did not trigger neuronal differentiation, but its co-expression with Ascl1 overcame the inhibition by Act Notch, as

Figure 3. MyT1 Binding Represses Neural Progenitor Genes

(A) Top overrepresented motifs in 50-bp regions centered at MyT1 peak summits are shown. Z, *Z* score; R, enrichment ratio.

(B) Frequency distribution of MyT1 motif centered at MyT1 peak summits (blue) or 2 kb upstream (control, gray). y axis represents the number of motifs in bins of 50 bp.

(C) Fold enrichment of MyT1 peaks with distinct number of MyT1 motifs as compared to control regions is shown.

(D) Number of MyT1 BEs associated with up- (blue bar) or downregulated (red bar) genes following a nearest gene annotation in MyT1 GoF DNA arrays. Statistical significance was assessed by comparing the association with 1,000 randomized datasets of equal size and assuming a normal distribution. Test data are represented as box with median of test and first and third quartiles. Whiskers, ±1.5× interquartile range (IQR).

(E) Heatmap displaying the cumulative fraction of deregulated genes in MyT1 GoF that are directly regulated by MyT1. Number of transcripts with expression FC > 1.2 are plotted against MyT1 BEs with increasing p value (bin = 94 BEs). Statistical significance was assessed by comparing the association with 100 randomly generated ChIP-seq datasets of equal size.

(F) ChIP-seq enrichment profiles of histone marks in undifferentiated NS5 cells, in 4-kb genomic regions centered at MyT1 peak summits. Dashed lines show the enrichment profile of histone marks at random genomic regions.

(G) Pie chart represents the fraction of MyT1 BE overlapping gene features.

(H) Heatmap representing the expression of MyT1 direct targets (bound and downregulated) in distinct layers of the E14.5 mouse embryonic telencephalon. Color code refers to relative gene expression levels. Hierarchical clustering was done using Pearson correlation. Absolute levels of expression of MyT1 are represented in the graph above. VZ, ventricular zone; SVZ, subventricular zone; CP, cortical plate.

(I) Absolute expression levels (fragments per kilobase per million mapped reads [FPKM]) of MyT1 direct targets in distinct layers of the E14.5 mouse embryonic telencephalon. Data distribution is represented as box with median and first and third quartiles (whiskers, ±1.5× IQR; notches, ±1.5× IQR/$n^{1/2}$).

(J) Enrichment of representative GO biological process terms associated with MyT1 targets (genes bound and downregulated by MyT1) is shown.

(K) Validation of MyT1 binding to selected genes by ChIP-qPCR with anti-HA antibody in NS5 cells upon MyT1 GoF is shown. ORF1 and ORF2, negative control regions. Mean ± SD of triplicate assays.

(L) Validation of gene expression changes of selected genes in NS5 cells 4 hr upon MyT1 GoF by expression qPCR is shown. Mean ± SD of triplicate assays.

(M) ChIP-qPCR using anti-LSD1 antibody in NS5 cells before (−Dox) and 4 hr after (+Dox) MyT1 GoF is shown. ORF1 and ORF2, negative control regions.

Data are shown as mean ± SD; n.s., $p > 0.05$; *$p < 0.05$, **$p < 0.01$, ***$p < 0.001$, and ****$p < 0.0001$, according to Student's t test (K–M). See also Figures S3 and S4.

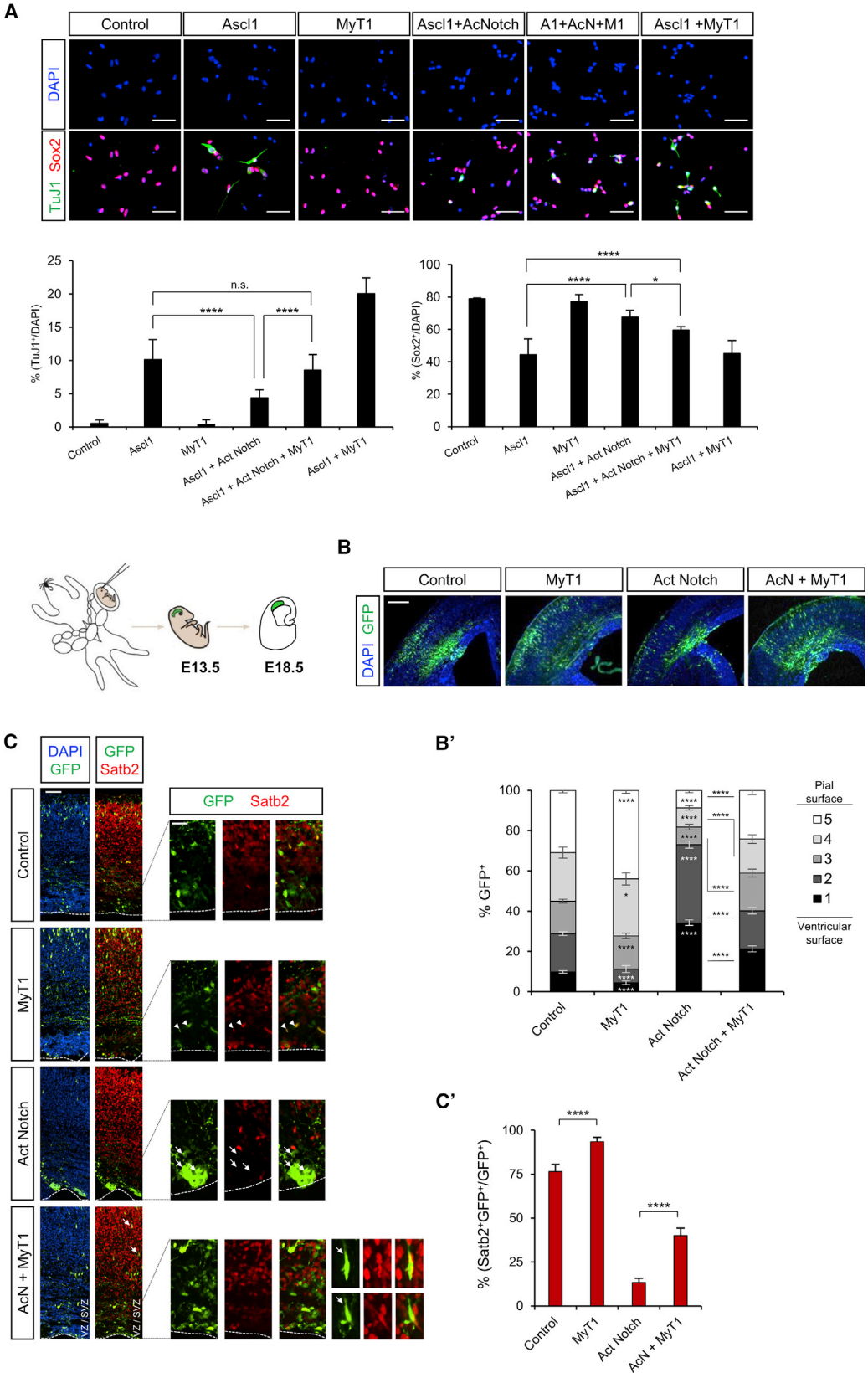

(legend on next page)

observed by a rescue of the number of TuJ1-positive cells to levels similar to those obtained with Ascl1 alone (with Sox2 expression following a similar trend). In addition, a strong increase in the differentiation activity of Ascl1 alone was observed when both factors (Ascl1 + MyT1) were co-expressed (Figures 4A and 4B, respectively). Altogether, our results suggest that MyT1 alone is not able to promote neuronal differentiation but that it enhances the activity of the proneural factor by counteracting the inhibitory activity of the Notch pathway.

We next tested whether MyT1 could similarly counteract Notch signaling in vivo by co-electroporating MyT1 and Act Notch expression vectors in the dorsal telencephalon. As expected, expression of Act Notch inhibited endogenous neurogenesis, resulting in the retention of electroporated cells closer to the ventricular surface and in a decreased number of cells expressing the neuronal marker Satb2 (Figures 4B and 4C), whereas MyT1 overexpression had the opposite effect (Figures 4B and 4C). Notably, co-expression of Act Notch and MyT1 rescued significantly the Act Notch phenotype (Figures 4B and 4C). Overall, these experiments support the conclusion that MyT1 counteracts Notch signaling during neurogenesis.

MyT1 Counteracts Notch Activation of Hes1 Expression

Considering the well-established role of Hes1 as a downstream effector of Notch signaling in neurogenesis (Artavanis-Tsakonas et al., 1999; Shimojo et al., 2008), we next focused on the regulation of this MyT1 target gene. Analysis of the MyT1 ChIP-seq profile showed strong enrichment at the *Hes1* proximal promoter region, centered on three evolutionarily conserved MyT1 motifs (Figure 5A). Strikingly, these motifs were found in tandem, and partially overlapping, with three Rbpj-binding motifs (TC box) previously shown to mediate the regulation of *Hes1* by Notch/Rbpj (Arnett et al., 2010; Jarriault et al., 1995; Nam et al., 2007) (Figure 5B). To test the ability of MyT1 to bind to its cognate motifs, we performed an electrophoretic mobility shift assay (EMSA) using a *Hes1* oligonucleotide probe spanning the MyT1 motifs or mutated versions. MyT1 was able to directly bind to this *Hes1* promoter probe, as shown by the formation of a large DNA/protein complex (Figure 5C). The formation of this complex was strongly reduced or abolished when each of the MyT1 motifs was disrupted separately or simultaneously, respectively, suggesting cooperative binding of MyT1 to the three sites.

We next investigated whether MyT1 could counteract the activity of Notch signaling on a luciferase reporter construct containing the *Hes1* proximal promoter region spanning all MyT1 and Rbpj sites (pHes1*::Luc*) (Nishimura et al., 1998). A transcriptional assay in transfected P19 cells showed Act Notch strongly activates the *Hes1* promoter, while co-expression of MyT1 completely abrogated this activity (Figure 5D). To test if the observed effect of MyT1 is dependent on DNA binding, we performed mutagenesis on the MyT1-binding sites. Mutations were designed so as to minimize any effect on Notch activation, resulting in promoter constructs that still responded, albeit less strongly, to Act Notch (Figure 5E). Disruption of individual binding sites partially impaired the activity of MyT1 (Figure 5F), while simultaneous disruption of the three sites (BS1 + 2 + 3) had a stronger effect readily observed when lower ratios of MyT1/Act Notch were used (Figure 5G). Similar results were obtained using a dominant active version of Rbpj fused to the VP16 activation domain (RBPJ-VP16) (Figure 5H), further supporting that MyT1 regulates *Hes1* at the promoter level. Importantly, no other transcription factor tested was able to counteract Act Notch activity on *Hes1* promoter (Figure S5). Altogether, we concluded that MyT1 counteracts the activity of the Notch/Rbpj complex on the *Hes1* promoter via a mechanism that depends on binding to the three MyT1-binding sites.

Next, we analyzed MyT1 protein and *Hes1* transcript expression patterns in the embryonic mouse telencephalon by double immuno/in situ hybridization, and we concluded these are largely non-overlapping (Figure 6A). To further investigate this with single-cell resolution, we re-examined the molecular signatures of 96 E11.5 dorsal telencephalic neural stem/progenitor cells obtained by single-cell RNA sequencing (RNA-seq) (Hagey and Muhr, 2014). Profiling using principal component 2 (PC2), which orders cells through differentiation according to markers that reflect the progression of cortical neurogenesis (Hagey and Muhr, 2014), showed an inverse correlation between *Myt1* and *Hes1* expression (Figure 6B, upper graph), with a Spearman correlation coefficient of reads per kilobase per million mapped reads (RPKM) levels of −0.407. In spite of this, examination of absolute RPKM levels showed that co-expression of both genes was detected in a small but significant fraction of cells, suggesting the onset of *Myt1* expression occurs in cells that still express *Hes1* (Figure 6B, bottom panel). Thus, *MyT1* expression is inversely correlated, but partially overlapping, with that of *Hes1*, which is consistent with MyT1 playing a determinant role in switching off *Hes1* transcription at the onset of neurogenesis.

MyT1 Represses Many Notch/Rbpj Transcriptional Targets

The overrepresentation of a putative Rbpj-binding motif at MyT1 target sites (Figure 3A) suggests the direct control of Notch target genes by MyT1 may extend beyond the regulation of *Hes1*. To investigate this, we compared the transcriptional

Figure 4. MyT1 Counteracts Inhibition of Neuronal Differentiation by Notch Signaling

(A) Immunocytochemical analysis of Sox2 (red) and TuJ1 (green) upon infection with control or Ascl1-, Act Notch-, and/or MyT1-inducible lentiviruses 48 hr post-Dox. Nuclei were labeled with DAPI (blue). Histograms represent the percentage of $Sox2^+$/DAPI or $TuJ1^+$/DAPI cells in each condition. Scale bar, 40 μm.

(B and C) In utero electroporation of control or MyT1, Act Notch, or Act Notch + MyT1 expression vectors in E13.5 mouse dorsal telencephalon. Immunofluorescence analysis of coronal sections of GFP (green) and the neuronal marker Satb2 (red) 5 days after electroporation (E18.5) is shown. Cell nuclei are labeled with DAPI (blue). Scale bars, 500 μm (B) and 50 and 20 μm (C, left and right). (B') Histogram represents the percentage of electroporated cells present in five bins (1 to 5 from ventricular to pial surface, respectively) of equal length spanning the cortical thickness. (C') Histogram represents the percentage of ($Satb2^+GFP^+$)/GFP^+ cells in each condition. Arrowheads indicate examples of $Satb2^+GFP^+$ cells. Arrows indicate examples of $Satb2^-GFP^+$ cells.

Data are shown as mean ± SD; n.s., $p > 0.05$; *$p < 0.05$, **$p < 0.01$, ***$p < 0.001$, and ****$p < 0.0001$, according to one-way ANOVA with Bonferroni correction for multiple testing (A) and Student's t test (B'–C').

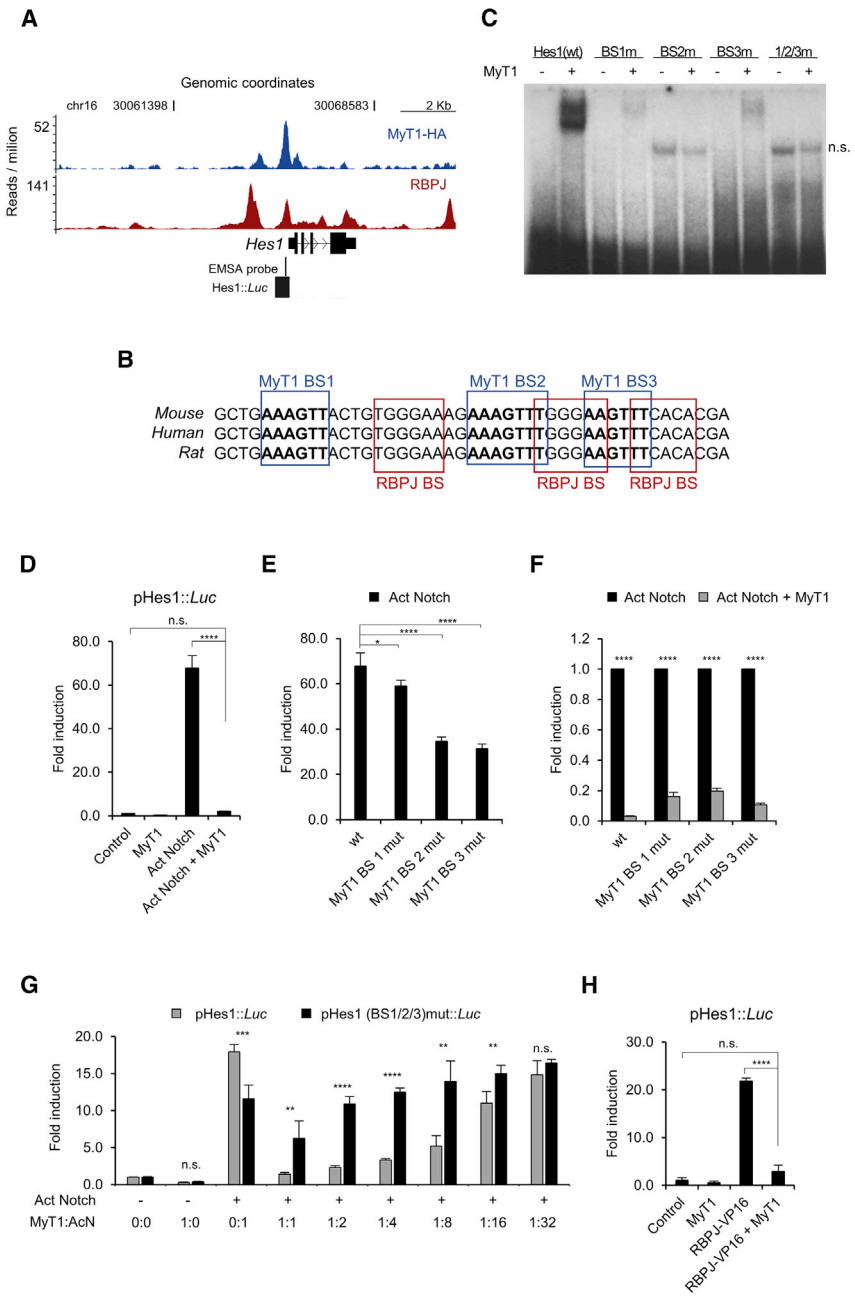

Figure 5. MyT1 Counteracts the Activity of Rbpj/Notch at the *Hes1* Promoter

(A) MyT1 (blue) and RBPJ (red) ChIP-seq enrichment profiles at the vicinity of *Hes1* gene. Regions contained in Hes1::*Luc* and EMSA probe are indicated below figure.

(B) Species alignment of *Hes1* proximal promoter region spanning MyT1 (blue) and Rbpj (red) binding motifs is shown.

(C) EMSA shows MyT1 binding to a *Hes1* promoter probe with wild-type (WT) sequence or mutations in MyT1 binding sites. n.s., non-specific band.

(D–G) Transcriptional assay in P19 cells co-transfected with control or MyT1 and/or Act Notch expression vectors and a reporter construct expressing luciferase under the control of *Hes1* proximal promoter region (pHes1::*Luc*) or mutated versions in which MyT1-binding sites were individually or simultaneously disrupted. Equal amounts of expression vectors were used, except in (G) in which the various MyT1:ActNotch ratios used are indicated. Mean ± SD of quadruplicate assays.

(H) Transcriptional assay in P19 cells co-transfected with a control or MyT1 and/or RBPJ-VP16 (Blanpain et al., 2006) expression vectors together with pHes1::*Luc* is shown.

Data are shown as mean ± SD; n.s., $p > 0.05$; *$p < 0.05$, **$p < 0.01$, ***$p < 0.001$, and ****$p < 0.0001$, according to Student's t test (F and G) or one-way ANOVA test with Bonferroni correction for multiple testing (D, E, and H). See also Figure S5.

changes observed in our MyT1 GoF model with those that take place upon exposure of NS5 cells to the pharmacological inhibitor of gamma-secretase LY411575 (LY), (Lanz et al., 2004), as assessed by RNA sequencing (RNA-seq) (Table S5). When considering a high-confidence list of genes deregulated upon MyT1 induction ($p < 0.01$, $n = 90$), the vast majority (81%) was also deregulated upon LY treatment, with all these but two genes changing in the same direction (Figure 7A). Notably, this same trend (expression of common deregulated genes changes in same direction) was maintained when decreasing the stringency cutoff for deregulation by MyT1 ($p < 0.05$, $n = 1,612$), or simultaneously increasing the stringency cutoff for deregulation upon LY treatment ($q < 0.01$, $n = 1,612$) (Figure 7A). Thus, MyT1 expression induces a global change in gene expression that resembles that triggered by the inhibition of Notch signaling.

Considering the short time points (4 hr) at which both expression profiling experiments were performed, it is likely that many genes downstream Notch are direct MyT1 targets. In agreement with this, we found a much stronger statistical association of MyT1 BEs with genes downregulated by LY than with upregulated ones ($p < 1.6 \times 10^{-70}$ versus $p < 1.1 \times 10^{-8}$) (Figure 7B). To evaluate the extent to which MyT1 represses genes directly activated by the Notch/Rbpj complex, we performed genome-wide mapping of Rbpj in NS5 cells by ChIP-seq, resulting in the identification of 15,281 BEs ($q < 10^{-2}$) (Table S6; Figure 7D) associated with 9,215 unique genes. As expected, a de novo search for DNA motifs enriched at Rbpj BEs found the TC box to be the most enriched motif, in addition to an E box (bHLH) and the compound Rfx/Rbpj motif (Figure 7C). A strong Rbpj-sequencing signal was found at genomic regions centered at MyT1 peak summits, confirming that MyT1 often binds in close vicinity to Rbpj (Figure 7E), as illustrated for several targets (Figures 5A and 7D). Notably, most (80.4%) of MyT1 direct targets identified were

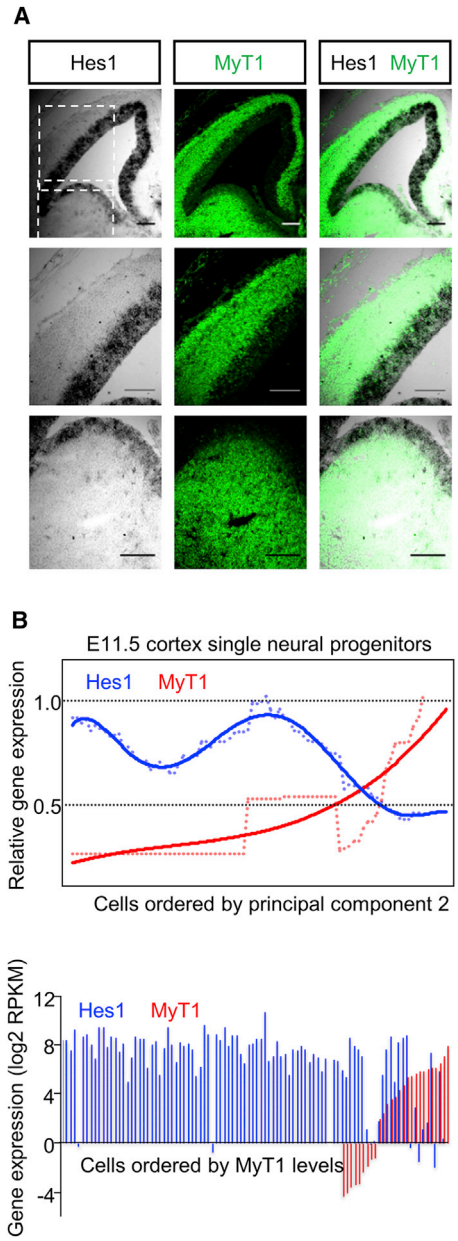

Figure 6. Comparative Analysis of MyT1 and Hes1 Expression in Neural Progenitor Cells

(A) Immunofluorescence of MyT1 (green) and in situ hybridization for Hes1 (gray) in frontal sections of E14.5 mouse embryonic telencephalon. Dashed squares indicate magnified regions of dorsal (middle) or ventral (bottom panels) domains. Scale bar, 140 μm.

(B) Top panel: relative expression of *Myt1* and *Hes1* in 96 E11.5 dorsal telencephalic neural progenitor cells, determined by single-cell RNA-seq. Dots represent rolling averages, ordered by principal component 2 (PC2), with polynomial trend lines overlapping. Bottom panel: absolute expression levels of *Myt1* and *Hes1* in neural progenitor cells are shown as above, ordered by MyT1 expression levels.

also bound by Rbpj. MyT1 and RBPJ binding and their opposite effects in target gene expression were validated for several genes (Figures 3K, 3L, 7F, and 7G). Most significantly was the ability of both pathways to oppositely regulate the expression of *Notch1*, further validated by the ability of MyT1 to counteract the activation of *Notch1* gene promoter by Act Notch in a transcriptional assay (Figures S6A–S6C). In conclusion, MyT1 can counteract the Notch pathway at distinct levels, repressing Notch-signaling components and many of its downstream targets.

DISCUSSION

In spite of its identification two decades ago, little progress has been made toward understanding the function of the zinc-finger factor MyT1 in vertebrate neurogenesis. After initial studies in *Xenopus* embryos suggested X-MyT1 promotes neurogenesis by counteracting lateral inhibition (Bellefroid et al., 1996), a confirmation of such model using mouse genetics has been hampered by functional redundancy with other family members (Wang et al., 2007). In addition, no molecular basis has been ever established for MyT1 function, to large extent due to the lack of identified target genes. Here we provide evidence of a neurogenic role for MyT1 in the developing mouse embryo, and we characterize its transcriptional program.

Activation of neuronal differentiation requires the concomitant repression of the gene expression program that operates in neural stem/progenitor cells, including the downregulation of the Notch transcriptional program (Imayoshi and Kageyama, 2014; Kageyama et al., 2008). This is often attributed to decreased Notch input signaling from neighboring cells (Kawaguchi et al., 2008; Nelson et al., 2013), which results in default repression of Notch target genes via the recruitment of corepressors by Rbpj. However, recent studies have reported that IPs exhibit attenuated Rbpj signaling as compared to RG cells, and they are unable to induce the expression of Hes genes upon activation of the Notch receptor (Kawaguchi et al., 2008; Mizutani et al., 2007; Nelson et al., 2013). This suggests the existence of cell-autonomous mechanisms to inhibit the Notch program at the onset of differentiation, which could be explained by the regulation of Notch target genes by transcription factors such as MyT1. In addition, MyT1 interacts with the Notch pathway also by regulating various pathway components. Most notably, the repression of *Notch1* receptor gene may lead to an overall decrease of Notch-signaling levels by MyT1. In agreement with this, the expression of *Hes5*, a well-established readout of Notch signaling, was strongly downregulated upon MyT1 expression with no apparent binding of MyT1 to its promoter region (Figures 3L, S6D, and S6E).

Among the targets identified, Hes1 is likely to be a major effector of MyT1 in neurogenesis. Hes1 expression intrinsically oscillates in proliferating neural stem/progenitor cells, by a mechanism that relies on its activation by Notch signaling. It is believed that the onset of differentiation depends critically on the sustained downregulation of Hes1 expression; however, the mechanisms that repress Hes1 in this context are poorly understood (Imayoshi and Kageyama, 2014; Imayoshi et al., 2013). The *cis* architecture of the *Hes1* promoter, where MyT1 and Rbpj sites are found interspersed and partially overlapping, was revealed to be a very efficient mechanism to counteract Notch activity. This feature may be unique to *Hes1*, as we did not find a similar *cis* architecture at other regulatory regions targeted by both pathways.

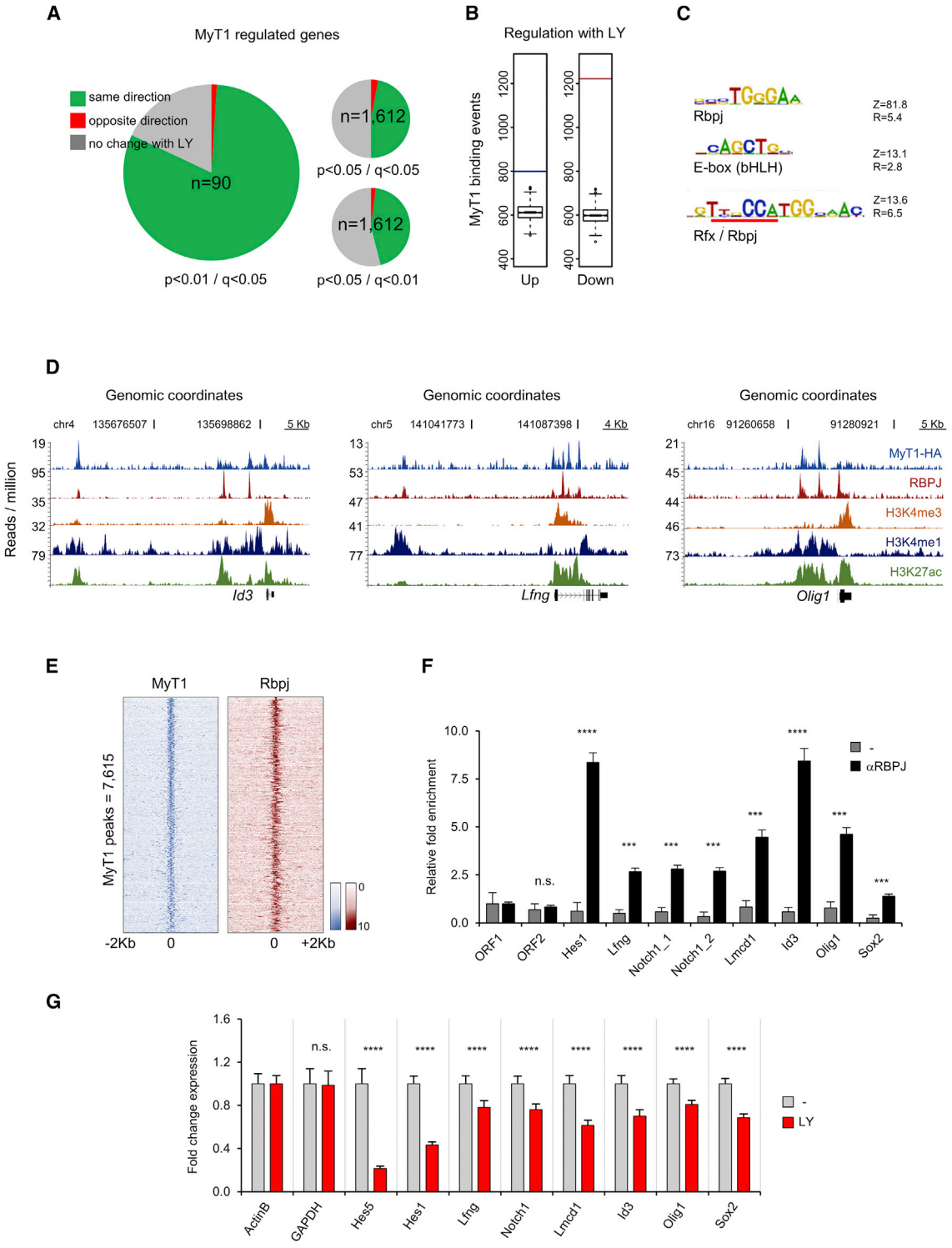

Figure 7. MyT1 and Notch Pathways Oppositely Regulate Many Transcriptional Targets

(A) Pie charts representing the percentage of genes deregulated in NS5 cells 4 hr upon MyT1 GoF and deregulated in the same direction (green), opposite direction (red), or unchanged/data unavailable (gray) 4 hr upon LY treatment. Cutoff values for analysis upon MyT1 GoF (p value) and exposure to LY (q value) are indicated in figure next to each pie chart. n, total number of genes.

(B) Number of MyT1 BEs associated with genes that are up- (blue bar) or downregulated (red bar) upon LY treatment. Boxplot distributions of MyT1-binding associations, which can be found testing against 1,000 different random sets of genes, are shown. Test data are represented as box with median of test and first and third quartiles (whiskers, ±1.5× IQR).

(legend continued on next page)

It has been shown that MyT1L cooperates with Ascl1 in reprogramming mouse embryonic fibroblasts (MEFs) into induced neurons (Vierbuchen et al., 2010). Although it is not clear what the levels of canonical Notch signaling are in MEFs, Hes1 expression is well documented in this cellular context. MyT1 family members have high sequence homology within the zinc-finger domains, and all have been shown to recognize the MyT1 DNA-binding motif (Bellefroid et al., 1996; Jiang et al., 1996; Yee and Yu, 1998). Therefore, it is possible that MyT1L functions, at least in part, by repressing Hes1 during reprogramming. In support of this, we found that MyT1L counteracts the Notch activation of *Hes1* promoter with the same efficiency as MyT1 (Figure S7A). In addition, ChIP-qPCR analysis of an HA-tagged version of MyT1L revealed a strong enrichment at *Hes1* proximal promoter soon after ectopic expression in MEFs (Figure S7B).

The broad expression of MyT1 in the embryonic nervous system (Matsushita et al., 2014), together with the importance of Notch signaling in neurogenesis, suggests that the regulatory events we identified in the telencephalon may occur pan-neuronally throughout the embryonic nervous system. In addition, while our study focuses on the function of MyT1 at the onset of neuronal differentiation, further research should also address the function of MyT1 at later stages along the neuronal lineage.

EXPERIMENTAL PROCEDURES

Immunohistochemistry and In Situ RNA Hybridization

Embryonic brains were processed for in situ hybridization or immunostaining as previously described (Castro et al., 2011). For double in situ hybridization/immunohistochemistry, frozen sections were treated as for in situ hybridization until the last post-fixation step, before immunostaining. The Hes1 probe was produced from the plasmid pBluescriptII SK-Hes1. NS5 cells were grown on glass coverslips coated with poly-L-Lysine (Sigma-Aldrich) and fixed with 4% formaldehyde for 10 min. See the Supplemental Experimental Procedures for antibody dilutions used. Bright-field and fluorescent images of fixed sections and coverslips were acquired using the microscope Leica DMRA2 or the laser-scanning confocal microscope Zeiss LSM510 Meta.

In Utero Electroporation

Mouse MyT1 cDNA (Nielsen et al., 2004) and AcNotch coding sequences were cloned upstream of an internal ribosomal entry site (IRES) and an nuclear localization signal (NLS)-tagged GFP in the pCAG expression vector (Niwa et al., 1991). Control and shRNA plasmids used (Sigma-Aldrich) were pLKO.1 scramble shRNA (Addgene 1864), pLKO MyT1 shRNA (TRCN0000081610), pLKO MyT1L shRNA (TRCN0000012109), and pLKO MyT3 shRNA (TRCN0000042479). Electroporation in utero was employed at E12.5 or E13.5 to deliver expression vectors (1 μl DNA plasmid corresponding to 3 μg mixed with 0.03% fast-green dye in PBS) to the ventricular RG cells of mouse embryos, as previously described (Saito, 2006; Sessa et al., 2008). All experiments were conducted upon the approval and following the guidelines of animal care and use committees from San Raffaele Scientific Institute (SRSI) and Instituto Gulbenkian de Ciência (IGC).

Culture and Infection of NS5 Cells

NS5 (Conti et al., 2005) and NS5-Ascl1-ERT2 cells (Raposo et al., 2015) were cultured in mouse Neurocult NSC basal medium supplemented with mouse Neurocult NSC proliferation supplement (STEMCELL Technologies), penicillin-streptomycin (100 U/mL) (Gibco), epidermal growth factor (EGF, 10 ng/mL) (PeproTech), basic FGF (10 ng/mL) (PeproTech), and laminin (1 μg/mL) (Sigma-Aldrich). For expression profiling and ChIP, NS5-MyT1-HA/GFP TetON cells were generated upon infection with MyT1-HA TetON-FUW, eGFP TetON-FUW, and M2rtTA TetON-FUW lentiviruses and were further expanded. When indicated, cells were treated with 50 nM Tam (Sigma-Aldrich), 2 μg/mL Dox hyclate (Sigma-Aldrich), or 10 nM LY (Lanz et al., 2004). Replication-incompetent lentiviruses were produced by transient transfection of HEK293T cells with TetON-FUW vectors co-transfected with psPAX2 and pCMV-VSVG. Lentiviral particles were concentrated from supernatant by ultracentrifugation at 9,000 × *g* for 4 hr and resuspended in 0.1% BSA PBS.

Gene Expression, DNA Microarrays, and RNA-Seq

Gene expression analysis of cultured NS5 cells by real-time qPCR with PerfeCTa SYBR Green FastMix, ROX (Quanta Biosciences) was carried out according to the manufacturer's instructions on an ABI7900 HT machine (Applied Biosystems), using cDNA produced with High Capacity RNA-to-cDNA Master Mix (Applied Biosystems) after Trizol RNA extraction (see the Supplemental Experimental Procedures for primers). Microarray analysis was performed on biological triplicates of NS5 MyT1-HA TetON cells 0 and 4 hr post-Dox induction. RNA concentration and purity were confirmed using Agilent 2100 Bioanalyzer with RNA Nano Kit (Agilent Technologies). RNA (100 ng) was processed with Ambion WT Expression Kit (Life Technologies) and hybridized to the Affymetrix Mouse Gene 1.0 ST Array. CEL files were analyzed using Chispter software (version 3.1.0, Kallio et al., 2011) using RNA normalization and empirical Bayes two-group test with Benjamini-Hochberg post hoc for p value correction. Samples used for RNA-seq analysis were obtained from biological triplicates of NS5 0 and 4 hr post-LY treatment, and total RNA was extracted as described above. The sequencing library was prepared according to the TruSeq RNA sample preparation version 2 protocol (Illumina) and sequenced on an Illumina HiSeq 2000. Raw reads were aligned to NCBI37 (mm9) mouse genome using Tophat2 version 2.0.3 (Kim et al., 2013). Pairwise analysis of differential gene expression was performed with cuffdiff version 2.1.1 using fragment bias and multi-read corrections (Trapnell et al., 2013). Genomic sequence and gene annotation were obtained from ENSEMBL (May 2012, version 67).

ChIP and ChIP-Seq

Ascl1 ChIP from embryonic telencephalon was performed as previously described (Castro et al., 2011). NS5 cells were fixed sequentially with 2 mM di(N-succimidyl) glutarate and 1% formaldehyde in PBS and lysed, sonicated, and immunoprecipitated as described previously (Castro et al., 2011), using anti-HA (ab1424, Abcam), anti-Rbpj (D10A4, Cell Signaling Technology), or anti-LSD1 (ab17721, Abcam) antibodies. DNA sequences were quantified by real-time PCR (see the Supplemental Experimental Procedures for primers). For sequencing, DNA libraries were prepared from 10 ng immunoprecipitated DNA according to the manufacturer's protocol. Paired-end sequencing was performed using MySeq. Raw reads were mapped to the mouse genome (NCBI37/mm9) with Bowtie version 0.12.7 (Langmead et al., 2009). Data were processed further with MACS version 1.4.1 (Zhang et al., 2008) to define the locations of BEs. Further details of data processing are described in the Supplemental Experimental Procedures.

(C) Top overrepresented motifs in 50-bp regions centered at MyT1 peak summits are shown. Z, *Z* score; R, enrichment ratio.
(D) Examples of MyT1 (blue) and RBPJ (red) ChIP-seq enrichment profiles at vicinity of common bound genes and associated H3K4me3 (orange), H3K4me1 (dark blue), and H3K27ac (green) ChIP-seq enrichment profiles are shown.
(E) Density plot of MyT1 (blue) and RBPJ (red) ChIP-seq reads at 4-kb genomic regions centered at MyT1 peak summits (signal intensity represents normalized tag count) is shown.
(F) Validation of RBPJ binding to selected genes by ChIP-qPCR in NS5 cells is shown. ORF1 and ORF2, negative control regions. Mean ± SD of triplicate assays.
(G) Validation of gene expression changes of selected genes in NS5 cells 4 hr after LY treatment by expression qPCR is shown.
Data are shown as mean ± SD; n.s., $p > 0.05$; *$p < 0.05$, **$p < 0.01$, ***$p < 0.001$, and ****$p < 0.0001$, according to Student's t test (F and G). See also Figure S6.

In Vitro Binding and Transcriptional Assays

EMSAs were performed as described previously (Castro et al., 2006), using probes (Supplemental Experimental Procedures) labeled with [γ-32P] ATP (PerkinElmer) using T4 polynucleotyde kinase (New England Biolabs). Control, MyT1, and RBPJ proteins produced by coupled in vitro transcription and translation in rabbit reticulocyte lysates (TNT, Promega) were incubated with probe in 20-μL binding reactions (15% glycerol, 20 mM HEPES [pH 7.9], 5 mM $MgCl_2$, 50 mM KCl, 0.1 mM $ZnSO_4$, 0.01% Triton X-100, 10 mM DTT, 5 mM PMSF, and 0.2 μg/uL herring sperm DNA; Sigma-Aldrich D7290) for 20 min at room temperature (RT). Reporter gene assays in transfected P19 cells were performed as previously described (Castro et al., 2011). Oligonucleotides used to mutate Hes1::*Luc* are described in the Supplemental Experimental Procedures.

Statistical Procedures

Where indicated, data from at least three (qPCR assays) or four (luciferase assays) biological replicates are presented as mean ± SD. For in utero electroporations, >500 cells from at least three sections were counted, using three embryos per condition. Differentiation in culture was scored counting >1,500 cells from three coverslips per condition. In all cases, statistical significance was calculated by performing a two-tailed, unpaired Student's t test or one-way ANOVA test with Bonferroni correction (see figure legends).

ACCESSION NUMBERS

The accession numbers for all genomic datasets reported in this paper are Array Express (http://www.ebi.ac.uk/arrayexpress): E-MTAB-4330 (MyT1 ChIP-seq), E-MTAB-4494 (Rbpj ChIP-seq in NS5 cells), E-MTAB-4335 (MyT1 GoF in NS5 cell DNA arrays), and E-MTAB-4331 (RNA-seq from NS5 cells treated with LY).

SUPPLEMENTAL INFORMATION

Supplemental Information includes Supplemental Experimental Procedures, seven figures, and twelve tables and can be found with this article online at http://dx.doi.org/10.1016/j.celrep.2016.09.024.

AUTHOR CONTRIBUTIONS

F.F.V. performed most experimental work with contributions from C.L. and D.M.T. V.T. performed the in vivo gene expression analysis and A.S. the in utero electroporation experiments. A.A.S.F.R. did most of the bioinformatics analysis with contributions from F.F.V. D.W.H. and J.M. performed the single-cell transcriptomics analysis. D.S.C., F.F.V., A.S., and V.B. designed experimental work. D.S.C. and F.F.V. wrote the manuscript, which was read and approved by all others.

ACKNOWLEDGMENTS

We thank the IGC Bioinformatics Unit for expert assistance in data analysis, the European Molecular Biology Laboratory (EMBL) Gene Core high-throughput sequencing Unit for ChIP-seq library preparation and sequencing, and the IGC Gene Expression Unit for DNA array processing and hybridization. We thank Guoqiang Gu for MyT1 and MyT1L antibodies; Brad G. Hoffman for the MyT3 antibody; and Ryoichiro Kageyama, Tasuku Honjo, Warren S. Pear, and Tohru Marunouchi for plasmids. This study was funded by Fundação para a Ciência e Tecnologia (FCT) grants UID/Multi/04555/2013 and PTDC/NEU-NMC/031572012 and Marie Curie CIG (303644) to D.S.C., the Telethon grant (GGP15096) and the Italian Ministry of Health Young investigator grant (GR-2013-02355540) to A.S., and an FCT doctoral fellowship (SFRH/BD/51178/2010) to F.F.V. D.S.C. is supported by the FCT Investigator program (IF/00413/2012).

Received: February 24, 2016
Revised: July 12, 2016
Accepted: September 9, 2016
Published: October 4, 2016

REFERENCES

Arnett, K.L., Hass, M., McArthur, D.G., Ilagan, M.X.G., Aster, J.C., Kopan, R., and Blacklow, S.C. (2010). Structural and mechanistic insights into cooperative assembly of dimeric Notch transcription complexes. Nat. Struct. Mol. Biol. *17*, 1312–1317.

Artavanis-Tsakonas, S., Rand, M.D., and Lake, R.J. (1999). Notch signaling: cell fate control and signal integration in development. Science *284*, 770–776.

Bai, G., Sheng, N., Xie, Z., Bian, W., Yokota, Y., Benezra, R., Kageyama, R., Guillemot, F., and Jing, N. (2007). Id sustains Hes1 expression to inhibit precocious neurogenesis by releasing negative autoregulation of Hes1. Dev. Cell *13*, 283–297.

Bellefroid, E.J., Bourguignon, C., Hollemann, T., Ma, Q., Anderson, D.J., Kintner, C., and Pieler, T. (1996). X-MyT1, a Xenopus C2HC-type zinc finger protein with a regulatory function in neuronal differentiation. Cell *87*, 1191–1202.

Berninger, B., Costa, M.R., Koch, U., Schroeder, T., Sutor, B., Grothe, B., and Götz, M. (2007). Functional properties of neurons derived from in vitro reprogrammed postnatal astroglia. J. Neurosci. *27*, 8654–8664.

Bertrand, N., Castro, D.S., and Guillemot, F. (2002). Proneural genes and the specification of neural cell types. Nat. Rev. Neurosci. *3*, 517–530.

Blanpain, C., Lowry, W.E., Pasolli, H.A., and Fuchs, E. (2006). Canonical notch signaling functions as a commitment switch in the epidermal lineage. Genes Dev. *20*, 3022–3035.

Castro, D.S., Skowronska-Krawczyk, D., Armant, O., Donaldson, I.J., Parras, C., Hunt, C., Critchley, J.A., Nguyen, L., Gossler, A., Göttgens, B., et al. (2006). Proneural bHLH and Brn proteins coregulate a neurogenic program through cooperative binding to a conserved DNA motif. Dev. Cell *11*, 831–844.

Castro, D.S., Martynoga, B., Parras, C., Ramesh, V., Pacary, E., Johnston, C., Drechsel, D., Lebel-Potter, M., Garcia, L.G., Hunt, C., et al. (2011). A novel function of the proneural factor Ascl1 in progenitor proliferation identified by genome-wide characterization of its targets. Genes Dev. *25*, 930–945.

Conti, L., Pollard, S.M., Gorba, T., Reitano, E., Toselli, M., Biella, G., Sun, Y., Sanzone, S., Ying, Q.-L., Cattaneo, E., and Smith, A. (2005). Niche-independent symmetrical self-renewal of a mammalian tissue stem cell. PLoS Biol. *3*, e283.

Englund, C., Fink, A., Lau, C., Pham, D., Daza, R.A., Bulfone, A., Kowalczyk, T., and Hevner, R.F. (2005). Pax6, Tbr2, and Tbr1 are expressed sequentially by radial glia, intermediate progenitor cells, and postmitotic neurons in developing neocortex. J. Neurosci. *25*, 247–251.

Farah, M.H., Olson, J.M., Sucic, H.B., Hume, R.I., Tapscott, S.J., and Turner, D.L. (2000). Generation of neurons by transient expression of neural bHLH proteins in mammalian cells. Development *127*, 693–702.

Fietz, S.A., Lachmann, R., Brandl, H., Kircher, M., Samusik, N., Schröder, R., Lakshmanaperumal, N., Henry, I., Vogt, J., Riehn, A., et al. (2012). Transcriptomes of germinal zones of human and mouse fetal neocortex suggest a role of extracellular matrix in progenitor self-renewal. Proc. Natl. Acad. Sci. USA *109*, 11836–11841.

Gaiano, N., Nye, J.S., and Fishell, G. (2000). Radial glial identity is promoted by Notch1 signaling in the murine forebrain. Neuron *26*, 395–404.

Gamsjaeger, R., Swanton, M.K., Kobus, F.J., Lehtomaki, E., Lowry, J.A., Kwan, A.H., Matthews, J.M., and Mackay, J.P. (2008). Structural and biophysical analysis of the DNA binding properties of myelin transcription factor 1. J. Biol. Chem. *283*, 5158–5167.

Gohlke, J.M., Armant, O., Parham, F.M., Smith, M.V., Zimmer, C., Castro, D.S., Nguyen, L., Parker, J.S., Gradwohl, G., Portier, C.J., and Guillemot, F. (2008). Characterization of the proneural gene regulatory network during mouse telencephalon development. BMC Biol. *6*, 15.

Gómez-López, S., Wiskow, O., Favaro, R., Nicolis, S.K., Price, D.J., Pollard, S.M., and Smith, A. (2011). Sox2 and Pax6 maintain the proliferative and developmental potential of gliogenic neural stem cells In vitro. Glia *59*, 1588–1599.

Götz, M., and Huttner, W.B. (2005). The cell biology of neurogenesis. Nat. Rev. Mol. Cell Biol. *6*, 777–788.

Hagey, D.W., and Muhr, J. (2014). Sox2 acts in a dose-dependent fashion to regulate proliferation of cortical progenitors. Cell Rep. *9*, 1908–1920.

Hu, J., Ho, A.L., Yuan, L., Hu, B., Hua, S., Hwang, S.S., Zhang, J., Hu, T., Zheng, H., Gan, B., et al. (2013). From the Cover: Neutralization of terminal differentiation in gliomagenesis. Proc. Natl. Acad. Sci. USA *110*, 14520–14527.

Hudson, L.D., Romm, E., Berndt, J.A., and Nielsen, J.A. (2011). A tool for examining the role of the zinc finger myelin transcription factor 1 (Myt1) in neural development: Myt1 knock-in mice. Transgenic Res. *20*, 951–961.

Imayoshi, I., and Kageyama, R. (2014). Oscillatory control of bHLH factors in neural progenitors. Trends Neurosci. *37*, 531–538.

Imayoshi, I., Isomura, A., Harima, Y., Kawaguchi, K., Kori, H., Miyachi, H., Fujiwara, T., Ishidate, F., and Kageyama, R. (2013). Oscillatory control of factors determining multipotency and fate in mouse neural progenitors. Science *342*, 1203–1208.

Jarriault, S., Brou, C., Logeat, F., Schroeter, E.H., Kopan, R., and Israel, A. (1995). Signalling downstream of activated mammalian Notch. Nature *377*, 355–358.

Jiang, Y., Yu, V.C., Buchholz, F., O'Connell, S., Rhodes, S.J., Candeloro, C., Xia, Y.R., Lusis, A.J., and Rosenfeld, M.G. (1996). A novel family of Cys-Cys, His-Cys zinc finger transcription factors expressed in developing nervous system and pituitary gland. J. Biol. Chem. *271*, 10723–10730.

Kageyama, R., Ohtsuka, T., Shimojo, H., and Imayoshi, I. (2008). Dynamic Notch signaling in neural progenitor cells and a revised view of lateral inhibition. Nat. Neurosci. *11*, 1247–1251.

Kallio, M.A., Tuimala, J.T., Hupponen, T., Klemelä, P., Gentile, M., Scheinin, I., Koski, M., Käki, J., and Korpelainen, E.I. (2011). Chipster: user-friendly analysis software for microarray and other high-throughput data. BMC Genomics *12*, 507.

Kawaguchi, A., Ikawa, T., Kasukawa, T., Ueda, H.R., Kurimoto, K., Saitou, M., and Matsuzaki, F. (2008). Single-cell gene profiling defines differential progenitor subclasses in mammalian neurogenesis. Development *135*, 3113–3124.

Kim, J.G., and Hudson, L.D. (1992). Novel member of the zinc finger superfamily: A C2-HC finger that recognizes a glia-specific gene. Mol. Cell. Biol. *12*, 5632–5639.

Kim, D., Pertea, G., Trapnell, C., Pimentel, H., Kelley, R., and Salzberg, S.L. (2013). TopHat2: accurate alignment of transcriptomes in the presence of insertions, deletions and gene fusions. Genome Biol. *14*, R36.

Kriegstein, A., and Alvarez-Buylla, A. (2009). The glial nature of embryonic and adult neural stem cells. Annu. Rev. Neurosci. *32*, 149–184.

Langmead, B., Trapnell, C., Pop, M., and Salzberg, S.L. (2009). Ultrafast and memory-efficient alignment of short DNA sequences to the human genome. Genome Biol. *10*, R25.

Lanz, T.A., Hosley, J.D., Adams, W.J., and Merchant, K.M. (2004). Studies of Abeta pharmacodynamics in the brain, cerebrospinal fluid, and plasma in young (plaque-free) Tg2576 mice using the gamma-secretase inhibitor N2-[(2S)-2-(3,5-difluorophenyl)-2-hydroxyethanoyl]-N1-[(7S)-5-methyl-6-oxo-6,7-dihydro-5H-dibenzo[b,d]azepin-7-yl]-L-alaninamide (LY-411575). J. Pharmacol. Exp. Ther. *309*, 49–55.

Louvi, A., and Artavanis-Tsakonas, S. (2006). Notch signalling in vertebrate neural development. Nat. Rev. Neurosci. *7*, 93–102.

Matsushita, F., Kameyama, T., and Marunouchi, T. (2002). NZF-2b is a novel predominant form of mouse NZF-2/MyT1, expressed in differentiated neurons especially at higher levels in newly generated ones. Mech. Dev. *118*, 209–213.

Matsushita, F., Kameyama, T., Kadokawa, Y., and Marunouchi, T. (2014). Spatiotemporal expression pattern of Myt/NZF family zinc finger transcription factors during mouse nervous system development. Dev. Dyn. *243*, 588–600.

Mikkelsen, T.S., Ku, M., Jaffe, D.B., Issac, B., Lieberman, E., Giannoukos, G., Alvarez, P., Brockman, W., Kim, T.-K., Koche, R.P., et al. (2007). Genome-wide maps of chromatin state in pluripotent and lineage-committed cells. Nature *448*, 553–560.

Mizutani, K., Yoon, K., Dang, L., Tokunaga, A., and Gaiano, N. (2007). Differential Notch signalling distinguishes neural stem cells from intermediate progenitors. Nature *449*, 351–355.

Nakada, Y., Hunsaker, T.L., Henke, R.M., and Johnson, J.E. (2004). Distinct domains within Mash1 and Math1 are required for function in neuronal differentiation versus neuronal cell-type specification. Development *131*, 1319–1330.

Nam, Y., Sliz, P., Pear, W.S., Aster, J.C., and Blacklow, S.C. (2007). Cooperative assembly of higher-order Notch complexes functions as a switch to induce transcription. Proc. Natl. Acad. Sci. USA *104*, 2103–2108.

Nelson, B.R., Hodge, R.D., Bedogni, F., and Hevner, R.F. (2013). Dynamic interactions between intermediate neurogenic progenitors and radial glia in embryonic mouse neocortex: potential role in Dll1-Notch signaling. J. Neurosci. *33*, 9122–9139.

Nielsen, J.A., Berndt, J.A., Hudson, L.D., and Armstrong, R.C. (2004). Myelin transcription factor 1 (Myt1) modulates the proliferation and differentiation of oligodendrocyte lineage cells. Mol. Cell. Neurosci. *25*, 111–123.

Nishimura, M., Isaka, F., Ishibashi, M., Tomita, K., Tsuda, H., Nakanishi, S., and Kageyama, R. (1998). Structure, chromosomal locus, and promoter of mouse Hes2 gene, a homologue of Drosophila hairy and Enhancer of split. Genomics *49*, 69–75.

Niwa, H., Yamamura, K., and Miyazaki, J. (1991). Efficient selection for high-expression transfectants with a novel eukaryotic vector. Gene *108*, 193–199.

Pang, Z.P., Yang, N., Vierbuchen, T., Ostermeier, A., Fuentes, D.R., Yang, T.Q., Citri, A., Sebastiano, V., Marro, S., Südhof, T.C., and Wernig, M. (2011). Induction of human neuronal cells by defined transcription factors. Nature *476*, 220–223.

Quan, X.-J., Denayer, T., Yan, J., Jafar-Nejad, H., Philippi, A., Lichtarge, O., Vleminckx, K., and Hassan, B.A. (2004). Evolution of neural precursor selection: functional divergence of proneural proteins. Development *131*, 1679–1689.

Raposo, A.A.S.F., Vasconcelos, F.F., Drechsel, D., Marie, C., Johnston, C., Dolle, D., Bithell, A., Gillotin, S., van den Berg, D.L.C., Ettwiller, L., et al. (2015). Ascl1 coordinately regulates gene expression and the chromatin landscape during neurogenesis. Cell Rep. *10*, 1544–1556.

Romm, E., Nielsen, J.A., Kim, J.G., and Hudson, L.D. (2005). Myt1 family recruits histone deacetylase to regulate neural transcription. J. Neurochem. *93*, 1444–1453.

Saito, T. (2006). In vivo electroporation in the embryonic mouse central nervous system. Nat. Protoc. *1*, 1552–1558.

Schneider, M.L., Turner, D.L., and Vetter, M.L. (2001). Notch signaling can inhibit Xath5 function in the neural plate and developing retina. Mol. Cell. Neurosci. *18*, 458–472.

Sessa, A., Mao, C.A., Hadjantonakis, A.K., Klein, W.H., and Broccoli, V. (2008). Tbr2 directs conversion of radial glia into basal precursors and guides neuronal amplification by indirect neurogenesis in the developing neocortex. Neuron *60*, 56–69.

Shimojo, H., Ohtsuka, T., and Kageyama, R. (2008). Oscillations in notch signaling regulate maintenance of neural progenitors. Neuron *58*, 52–64.

Trapnell, C., Hendrickson, D.G., Sauvageau, M., Goff, L., Rinn, J.L., and Pachter, L. (2013). Differential analysis of gene regulation at transcript resolution with RNA-seq. Nat. Biotechnol. *31*, 46–53.

Vasconcelos, F.F., and Castro, D.S. (2014). Transcriptional control of vertebrate neurogenesis by the proneural factor Ascl1. Front. Cell. Neurosci. *8*, 412.

Vierbuchen, T., Ostermeier, A., Pang, Z.P., Kokubu, Y., Südhof, T.C., and Wernig, M. (2010). Direct conversion of fibroblasts to functional neurons by defined factors. Nature *463*, 1035–1041.

Wang, S., Zhang, J., Zhao, A., Hipkens, S., Magnuson, M.A., and Gu, G. (2007). Loss of Myt1 function partially compromises endocrine islet cell differentiation and pancreatic physiological function in the mouse. Mech. Dev. *124*, 898–910.

Wang, S., Hecksher-Sorensen, J., Xu, Y., Zhao, A., Dor, Y., Rosenberg, L., Serup, P., and Gu, G. (2008). Myt1 and Ngn3 form a feed-forward expression loop to promote endocrine islet cell differentiation. Dev. Biol. *317*, 531–540.

Wilkinson, G., Dennis, D., and Schuurmans, C. (2013). Proneural genes in neocortical development. Neuroscience *253*, 256–273.

Yee, K.S., and Yu, V.C. (1998). Isolation and characterization of a novel member of the neural zinc finger factor/myelin transcription factor family with transcriptional repression activity. J. Biol. Chem. *273*, 5366–5374.

Yokoyama, A., Igarashi, K., Sato, T., Takagi, K., Otsuka I, M., Shishido, Y., Baba, T., Ito, R., Kanno, J., Ohkawa, Y., et al. (2014). Identification of myelin transcription factor 1 (MyT1) as a subunit of the neural cell type-specific lysine-specific demethylase 1 (LSD1) complex. J. Biol. Chem. *289*, 18152–18162.

Zhang, Y., Liu, T., Meyer, C.A., Eeckhoute, J., Johnson, D.S., Bernstein, B.E., Nusbaum, C., Myers, R.M., Brown, M., Li, W., and Liu, X.S. (2008). Model-based analysis of ChIP-Seq (MACS). Genome Biol. *9*, R137.

Cell Reports, Volume *17*

Supplemental Information

MyT1 Counteracts the Neural Progenitor Program to Promote Vertebrate Neurogenesis

Francisca F. Vasconcelos, Alessandro Sessa, Cátia Laranjeira, Alexandre A.S.F. Raposo, Vera Teixeira, Daniel W. Hagey, Diogo M. Tomaz, Jonas Muhr, Vania Broccoli, and Diogo S. Castro

MyT1 expression in Ascl1 LoF and GoF microarrays				
		Linear FC	P value	Reference
Ascl1 LoF	NS cells	-5.00	4.56×10^{-2}	Table S7 on Castro et al., 2011
	Telencephalon	-2.99	1.46×10^{-4}	Table S2 on Castro et al., 2011
Ascl1 GoF	NS cells	7.08	5.76×10^{-5}	Table S1 on Raposo et al., 2015
	Telencephalon	1.47	2.28×10^{-2}	Gohlke et al., 2008 Table S3 on Castro et al., 2011

Figure S1. MyT1 expression data from Ascl1 GoF and LoF experiments in mouse embryonic telencephalon and in cultured NS cells (related to Figure 1)
Ascl1 LoF in telencephalon, DNA arrays on RNA extracted from E13.5 ventral telencephalon of wild-type and Ascl1 knock-out mice (Castro et al. 2011). Ascl1 GoF in telencephalon, DNA arrays on RNA extracted from In utero electroporated E10.5 mouse telencephalon with control or Ascl1-expressing vectors (Castro et al., 2011; Gohlke et al., 2008). Ascl1 LoF in NS cells, DNA arrays on RNA extracted from NS5 cells electroporated with control or bHLH domain of Ascl1 fused to EnR domain expressing vectors (Castro et al., 2011). Ascl1 GoF in NS cells, DNA arrays on NS5 Ascl1-ERT2 cells before and after Tam induction (Raposo et al., 2015). FC, Fold Change.

Figure S2

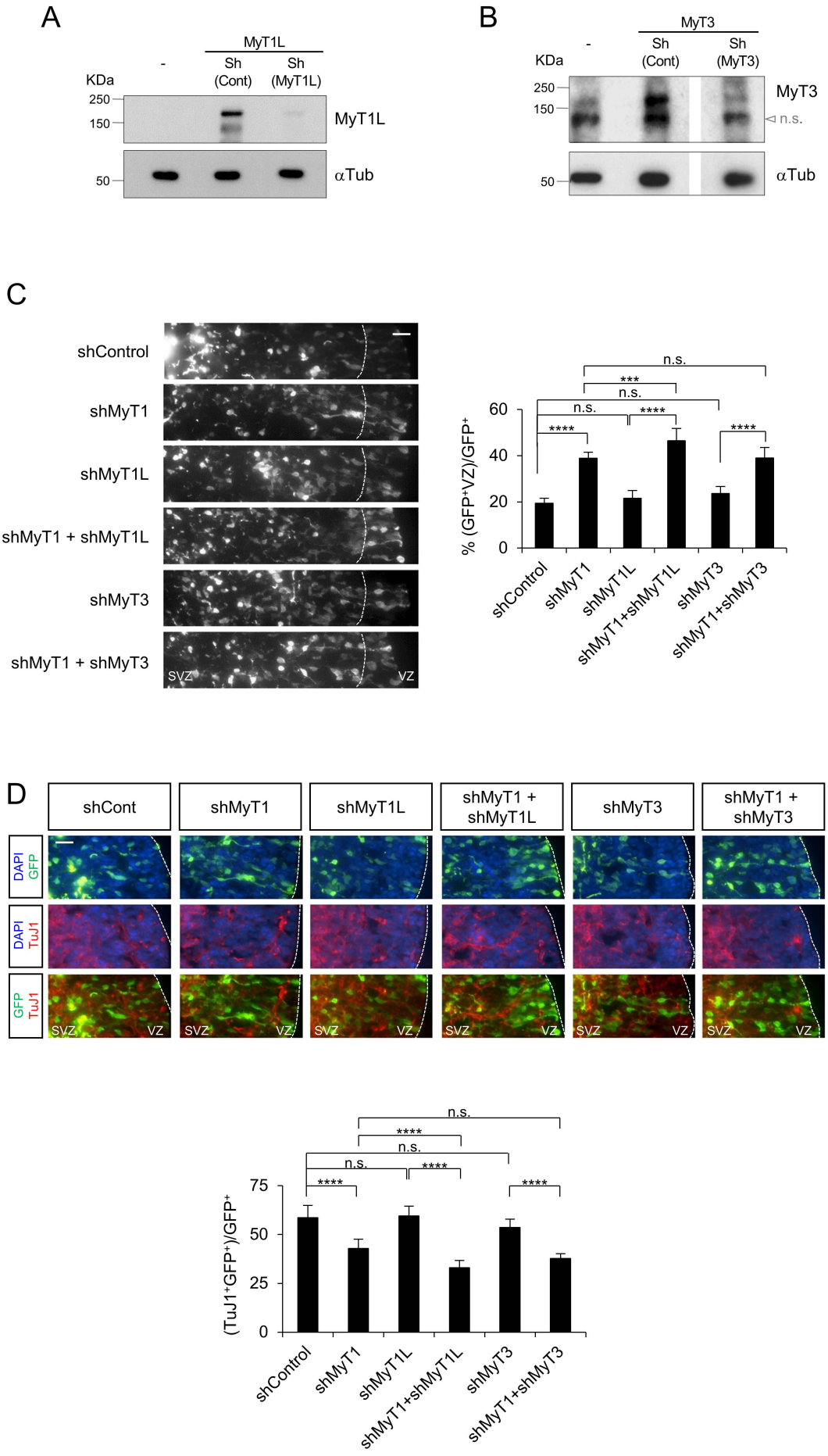
A
MyT1L
-
Sh (Cont)
Sh (MyT1L)
KDa
250
150
50
MyT1L
αTub
B
MyT3
-
Sh (Cont)
Sh (MyT3)
KDa
250
150
50
MyT3
n.s.
αTub
C
shControl
shMyT1
shMyT1L
shMyT1 + shMyT1L
shMyT3
shMyT1 + shMyT3
SVZ
VZ
% (GFP+VZ)/GFP+
n.s.
***
n.s.
n.s.
****
****
****
60
40
20
0
shControl
shMyT1
shMyT1L
shMyT1+shMyT1L
shMyT3
shMyT1+shMyT3
D
shCont
shMyT1
shMyT1L
shMyT1 + shMyT1L
shMyT3
shMyT1 + shMyT3
DAPI GFP
DAPI TuJ1
GFP TuJ1
SVZ
VZ
(TuJ1+GFP+)/GFP+
n.s.
****
n.s.
n.s.
****
****
****
75
50
25
0
shControl
shMyT1
shMyT1L
shMyT1+shMyT1L
shMyT3
shMyT1+shMyT3

Figure S2. Combined knock-down of MyT1 family members by in utero electroporation in ventral telencephalon (related to Figure 2)
Analysis by Western blot of MyT1L **(A)** or MyT3 **(B)** protein levels in P19 cells co-transfected with scramble shRNA (shControl), MyT1L ShRNA (shMyT1L) **(A)** or MyT3 ShRNA (shMyT3) **(B)**. α-tubulin was used as loading control. n.s.: non-specific band. **(C-D)** In utero electroporation of control (shControl), MyT1 (shMyT1), MyT1L (shMyT1L) and/or MyT3 (shMyT3) ShRNA vectors in E12.5 mouse ventral telencephalon. Immunofluorescence analysis on coronal section of the telencephalon for GFP (green or grey) and TuJ1 (red) 2 days post electroporation (E14.5). Cell nuclei are labeled with DAPI (blue). Scale bars, 20μm and 50μm (C and D). VZ: ventricular zone, SVZ: subventricular zone. Histograms represent the quantification of cell migration based on the fraction of GFP^+ cells that are retained in the VZ (GFP^+VZ/GFP^+) **(C)** and of neuronal differentiation based on the fraction of GFP^+ cells that express TuJ1 (($TuJ1^+GFP^+$)/GFP^+) **(D).** Mean ± SD. n.s. for P>0.05,* for P<0.05, ** for P<0.01, *** for P<0.001, **** for P<0.0001 according to one-way ANOVA with Bonferroni correction for multiple testing.

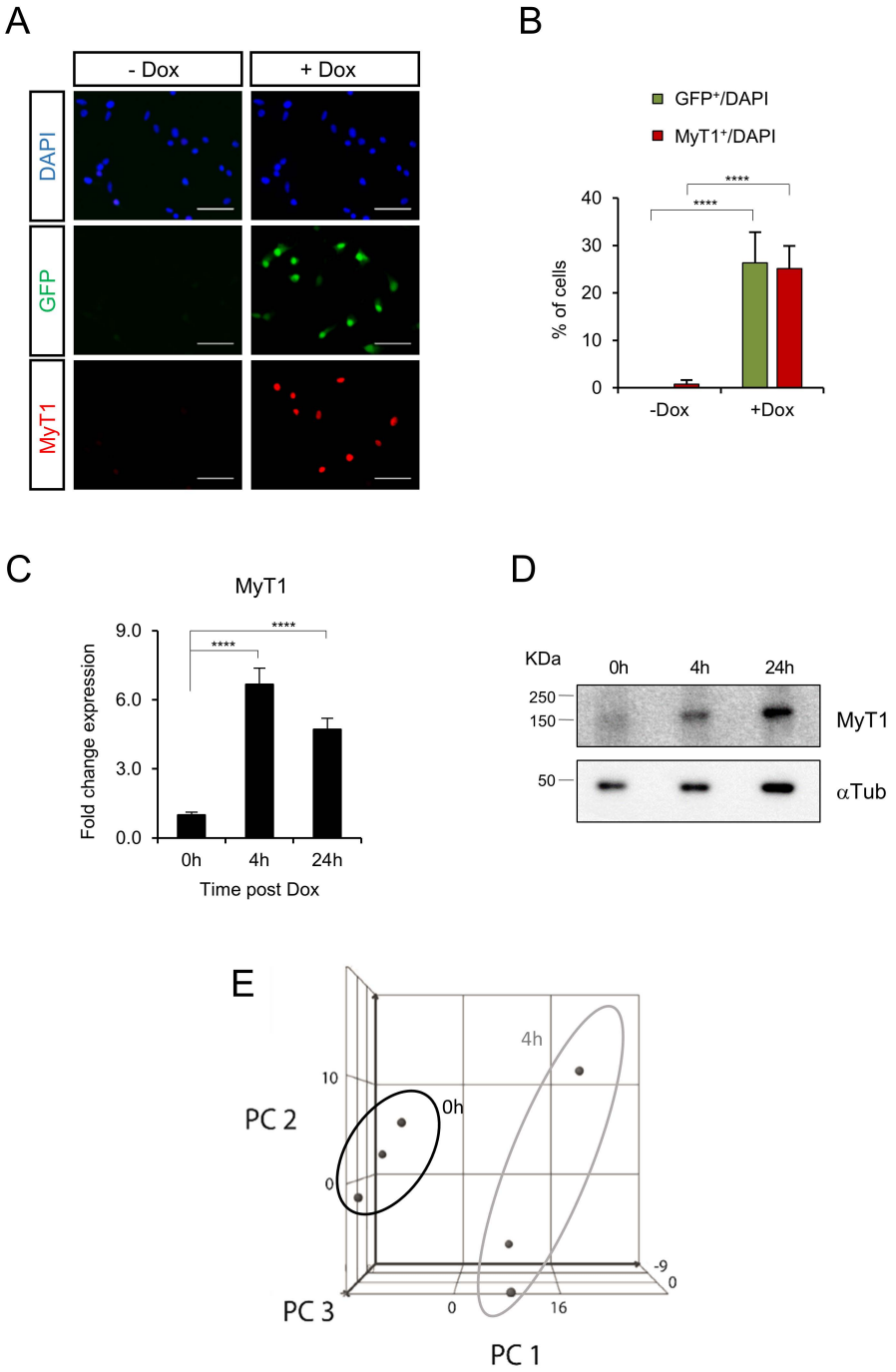

Figure S3. MyT1 GoF in NS5 cells using a Dox-inducible system (related to Figure 3) **(A)** Immunocytochemistry analysis for MyT1 (red) and GFP (green) before (-Dox) and 24h post Dox (+Dox) addition to NS5 MyT1-HA inducible cell cultures. Nuclei were stained with DAPI (blue). Scale bar, 40µm. **(B)** Histogram represents the percentage of GFP$^+$ cells (GFP$^+$/DAPI) and of MyT1 overexpressing cells (MyT1$^+$/DAPI). Mean ± SD for at least 1000 cells on each condition. **** for P<0.0001 according to Student's t-test. **(C)** Analysis of MyT1 RNA expression by qPCR. Mean ± SD of triplicate assays. **** for P<0.0001 according to one-way ANOVA test with Bonferroni correction for multiple testing. **(D)** Analysis of MyT1 protein levels by Western blot post-Dox induction. α-tubulin was used as loading control. **(E)** Principal component analysis (PCA) of technical replicates of MyT1 GoF gene expression DNA arrays 0h and 4h post Dox.

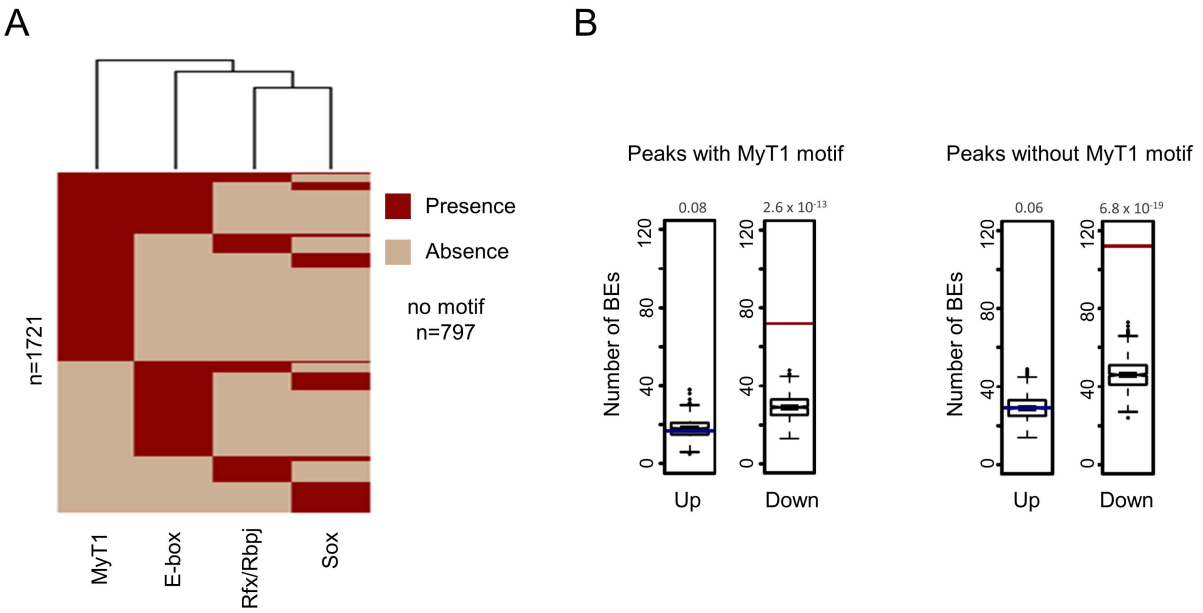

Figure S4. DNA binding motif analysis of MyT1 binding (related to Figure 3)
(A) Hierarchical clustering of MyT1 peaks based on the presence (red) or absence (tan) of MyT1, E-box, RFX and Sox motifs. **(B)** Number of MyT1 BEs containing (left) or not containing (right) MyT1 motif associated with up- (blue bar) or downregulated (red bar) genes in MyT1 GoF DNA arrays. Test data represented as box with median of test and 1st and 3rd quartiles; whiskers, ±1.5xIQR. P-values are indicated above each box.

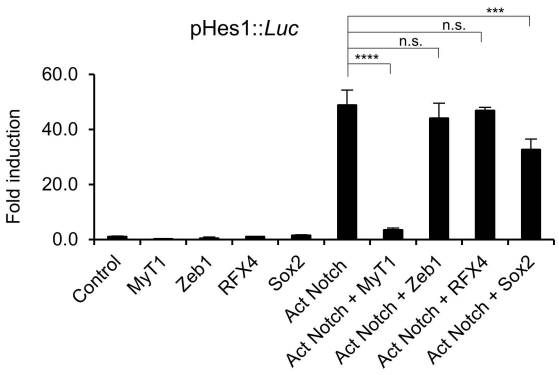

Figure S5. Control experiments demonstrating specificity of MyT1 inhibition of *Hes1* promoter (related to Figure 5)

Transcriptional assay in P19 cells co-transfected with control, MyT1, Zeb1, RFX4, Sox2 and/or Act Notch expression vectors and pHes1*::Luc*. Mean ± SD of quadruplicate assays. n.s. for P>0.05, *** for P<0.001, **** for P<0.0001 according to one-way ANOVA test with Bonferroni correction for multiple testing.

Figure S6

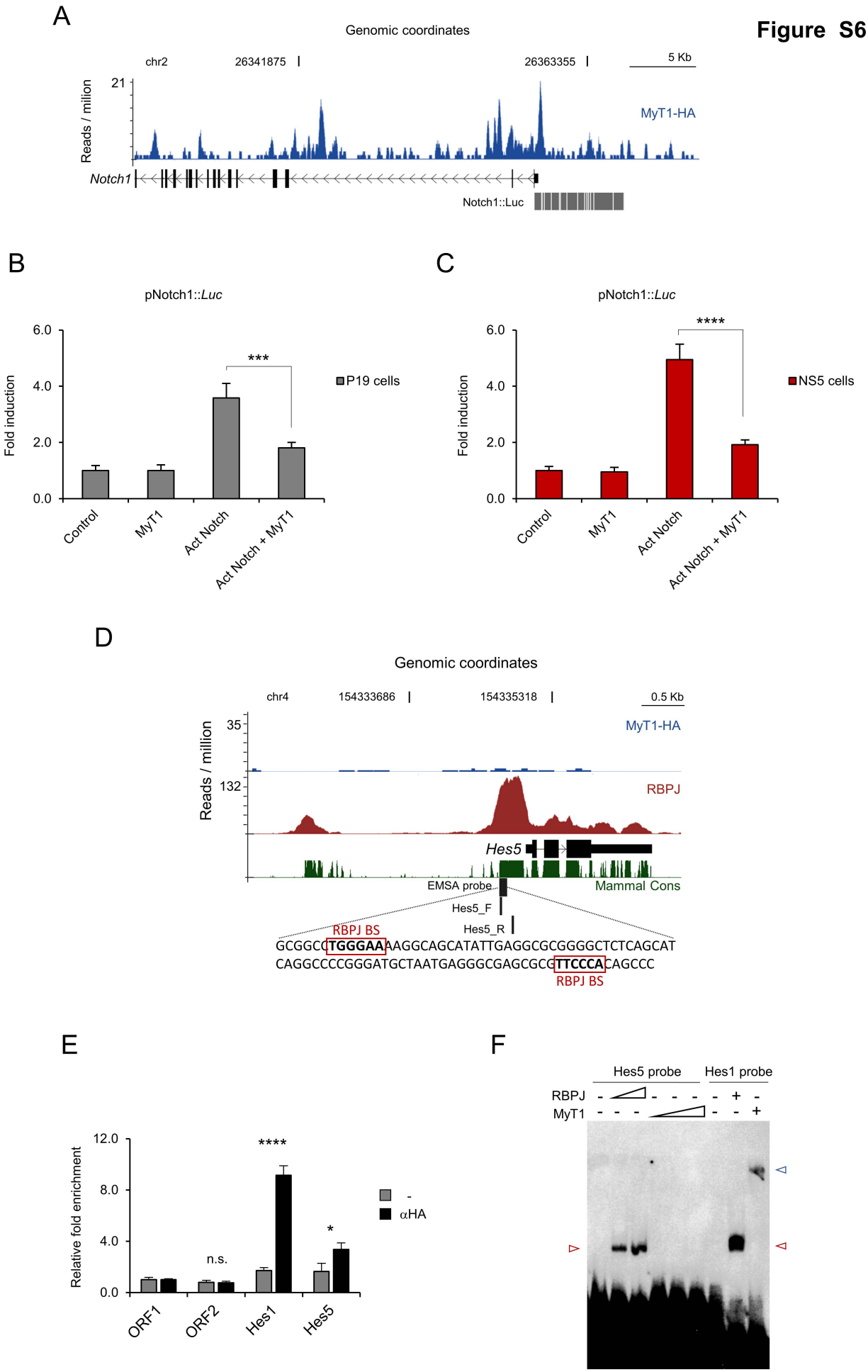
A
Genomic coordinates
chr2
26341875
26363355
5 Kb
Reads / milion
21
MyT1-HA
Notch1
Notch1::Luc
B
pNotch1::Luc
Fold induction
6.0
4.0
2.0
0.0
***
P19 cells
Control
MyT1
Act Notch
Act Notch + MyT1
C
pNotch1::Luc
****
NS5 cells
D
Genomic coordinates
chr4
154333686
154335318
0.5 Kb
35
132
MyT1-HA
RBPJ
Hes5
EMSA probe
Mammal Cons
Hes5_F
Hes5_R
RBPJ BS
GCGGCCTGGGAAAAGGCAGCATATTGAGGCGCGGGGCTCTCAGCAT
CAGGCCCCGGGATGCTAATGAGGGCGAGCGCGTTCCCACAGCCC
RBPJ BS
E
Relative fold enrichment
12.0
8.0
4.0
0.0
****
*
n.s.
-
αHA
ORF1
ORF2
Hes1
Hes5
F
Hes5 probe
Hes1 probe
RBPJ
MyT1

Figure S6. Analysis of MyT1 binding and regulation of *Notch1* and *Hes5* regulatory regions (related to Figure 7)

(A) MyT1 ChIP-Seq enrichment profiles at vicinity of *Notch1* gene. Genomic region contained in pNotch1*::Luc* (Yashiro-Ohtani et al., 2009) is indicated below figure; white vertical bars represent the position of MyT1 motifs. **(B-C)** Transcriptional assays in P19 cells **(B)** and NS5 cells **(C)** co-transfected with control, MyT1 and/or Act Notch expression vectors and a reporter construct expressing luciferase under the control of *Notch1* proximal promoter region pNotch1*::Luc.* Mean ± SD of quadruplicate assays. **(D)** MyT1 (blue) and RBPJ (red) ChIP-Seq enrichment profiles at vicinity of Hes5 gene. Genomic location of the ChIP-qPCR primers (Hes5_F, Hes5_R) and EMSA probe are indicated. Sequence of *Hes5* EMSA probe and position of RBPJ BSs are indicated below. Green track, Mammal conservation by PhastCons. **(E)** ChIP-qPCR using an anti-HA antibody in NS5 cells upon MyT1 GoF. ORF1 and ORF2, negative control regions. Mean ± SD of triplicate assays. **(F)** EMSA testing MyT1 binding to *Hes5* probe. *Hes1* promoter probe and RBPJ-expressing reticulocytes were used as positive controls. Blue arrowhead indicates MyT1 binding to *Hes1* probe. Red arrowheads indicate RBPJ binding to *Hes1* and *Hes5* probes. Different exposure times for different parts of the same gel are shown. n.s. for $P>0.05$,* for $P<0.05$, *** for $P<0.001$, **** for $P<0.0001$ according to Student's t-test **(C,E)**.

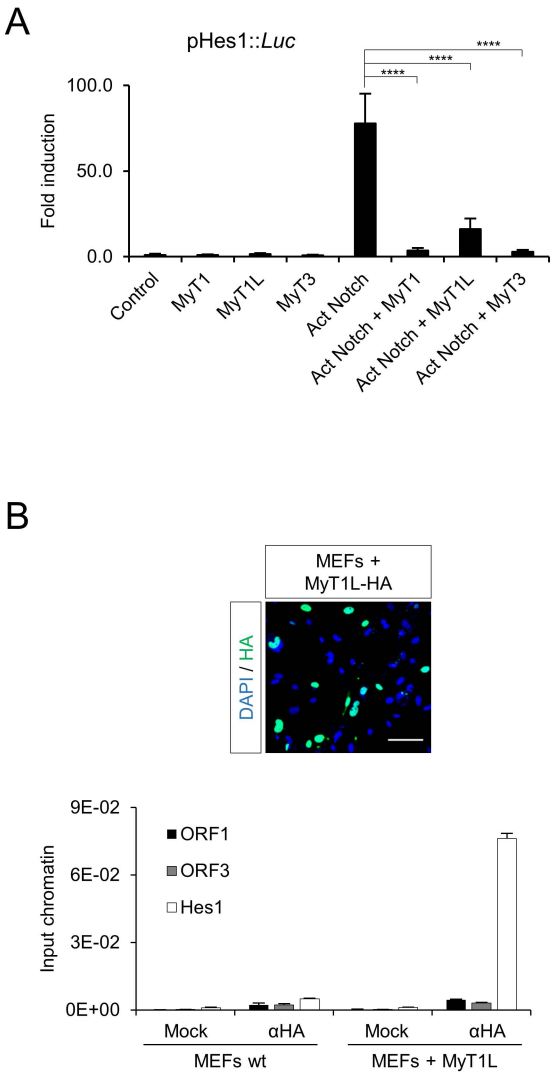

Figure S7. Functional conservation of Hes1 regulation by MyT1 family members (related to Figure 5)

(A) Transcriptional assay in P19 cells co-transfected with control, MyT1, MyT1L, MyT3 and/or Act Notch expression vectors and pHes1*::Luc*. Mean ± SD of quadruplicate assays. **** for P<0.0001 according to one-way ANOVA test with Bonferroni correction for multiple testing.

(B) Top panel: immunocytochemical analysis with anti-HA in MEFs 48h upon infection with a MyT1L-HA-expressing lentivirus. Bottom panel: analysis of MyT1L-HA binding in the *Hes1* proximal promoter region by ChIP-qPCR in chromatin extracted from MEFs wild-type (not infected) and MEFs MyT1L-HA (48h upon infection). ORF1 and ORF3, negative control regions. Mean ± SD of triplicate assays.

List of Supplemental Tables

Table S1. Genes deregulated 4h after MyT1 GoF in NS5 cells (related to Figure 3).

Table S2. Genomic coordinates of MyT1-HA binding events determined by ChIP-Seq (related to Figure 3).

Table S3. Genes bound and repressed by MyT1 GoF (related to Figure 3).

Table S4. Identity of MyT1 target genes associated with enriched Gene Ontology terms (related to Figure 3)

Table S5. Expression profiling dataset upon Notch inhibition (related to Figure 5).

Table S6. Genomic coordinates of RBPJ binding events determined by ChIP-Seq (related to Figure 7).

Supplemental experimental procedures

1. Plasmids

pCAG-MyT1-IRES-GFP
The full-length cDNA of mouse MyT1 was excised from pMycMyT1-7ZF-IRES/Red vector with EcoRI and subcloned (blunt ended) into the EcoRV site of pCAG-LinkerA-IRES-NLS-GFP.

MyT1-HA TetON-FUW
An HA-tag encoding oligonucleotide with restriction sites for XhoI and NotI at each end and EcoRI and AgeI sites downstream the HA-tag was inserted into the XhoI and NotI sites of pPyCAG-MCS-MyT1-V5. The ECoRI fragment of MyT1-V5 was subcloned into the EcoRI site of TetON-FUW.

FLAG-Act Notch TetON-FUW
Activated Notch1 tagged N-terminally with FLAG-tag was excised from pCAG-IRES-GFP-FLAG-Act Notch with BamHI, and cloned upon Klenow fill in reaction into the EcoR1 site of TetON-FUW.

MyT1L-HA TetON-FUW
An HA-tag oligonucleotide was inserted into the pCAG-MyT1L by PCR amplification using primers containing the HA-tag, STOP codon, one EcoRI site and one BglII site. The amplified fragment and the pCAG-MyT1L were digested with SacI and BglII. MyT1L-HA was excised from pCAG-MyT1L-HA vector using EcoRI and cloned into TetON-FUW.

Site-directed mutagenesis of pHes1*::Luc*
The mutations on the MyT1 BSs on the Hes1 promoter luciferase reporter (pHes1*::Luc*) were generated by site-directed mutagenesis using the plasmid pHes1*::Luc* and the primers listed on the Table S7. PCR reactions were performed with 50nM of each

primer, 100ng of plasmid, 100µM dNTPs, 7.5U of Cloned Pfu polymerase and Pfu buffer with $MgSO_4$ (Stratagene). Reaction was run under the following cycling conditions: 1 cycle 95ºC/5min; 18 cycles (95ºC/50sec; 60ºC/50sec; 72ºC/10min); 1 cycle 72ºC/25min, followed by treatment with DpnI for 3-4h at 37ºC.

Table S7 Oligonucleotides used for site-directed mutagenesis of pHes1*::Luc* (related to Figure 5)

Primer	Sequence
MyT1_BS1_mut_FW	CTCTTCCTCCCATTGGCTGAACCCTACTGTGGGAAAGAAAGTTTG
MyT1_BS1_mut_RV	CAAACTTTCTTTCCCACAGTAGGGTTCAGCCAATGGGAGGAAGAG
MyT1_BS2_mut_FW	GAAAGTTACTGTGGGAAAGAACCATTGGGAAGTTTCACACGAGCC
MyT1_BS2_mut_RV	GGCTCGTGTGAAACTTCCCAATGGTTCTTTCCCACAGTAACTTTC
MyT1_BS3_mut_FW	GAAAGAAAGTTTGGGAACCTTCACACGAGCCGTTCG
MyT1_BS3_mut_RV	CGAACGGCTCGTGTGAAGGTTCCCAAACTTTCTTTC
MyT1_BS1+2+3_mut_FW	GAAAGAACCATTGGGAACCTTCACACGAGCCGTTC
MyT1_BS1+2+3_mut_RV	GAACGGCTCGTGTGAAGGTTCCCAATGGTTCTTTC

2. Electromobility shift assay

Table S8 Oligonucleotides used as EMSA probes (related to Figure 5)

EMSA probe primers	Sequence
Hes1_WT_F	TGGCTGAAAGTTACTGTGGGAAAGAAAGTTTGGGAAGTTTCACACGAGCC
Hes1_WT_R	GGCTCGTGTGAAACTTCCCAAACTTTCTTTCCCACAGTAACTTTCAGCCA
Hes1_MyT1_BS1_mut_F	TGGCTGAACCCTACTGTGGGAAAGAAAGTTTGGGAAGTTTCACACGAGCC
Hes1_MyT1_BS1_mut_R	GGCTCGTGTGAAACTTCCCAAACTTTCTTTCCCACAGTAGGGTTCAGCCA
Hes1_MyT1_BS2_mut_F	TGGCTGAAAGTTACTGTGGGAAAGAACCATTGGGAAGTTTCACACGAGCC
Hes1_MyT1_BS2_mut_R	GGCTCGTGTGAAACTTCCCAATGGTTCTTTCCCACAGTAACTTTCAGCCA
Hes1_MyT1_BS3_mut_F	TGGCTGAAAGTTACTGTGGGAAAGAAAGTTTGGGAACCTTCACACGAGCC
Hes1_MyT1_BS3_mut_R	GGCTCGTGTGAAGGTTCCCAAACTTTCTTTCCCACAGTAACTTTCAGCCA
Hes1_MyT1_BS1+2+3_mut_F	TGGCTGAACCCTACTGTGGGAAAGAACCATTGGGAACCTTCACACGAGCC
Hes1_MyT1_BS1+2+3_mut_R	GGCTCGTGTGAAGGTTCCCAATGGTTCTTTCCCACAGTAGGGTTCAGCCA
Hes5_F	GCGGCCTGGGAAAAGGCAGCATATTGAGGCGCGGGGCTCTCAGCATCAGGCCCCGGGATGCTAATGAGGGCGAGCGCGTTCCCACAGCCC
Hes5_R	GGGCTGTGGGAACGCGCTCGCCCTCATTAGCATCCCGGGGCCTGATGCTGAGAGCCCCGCGCCTCAATATGCTGCCTTTTCCCAGGCCGC

3. Expression q-PCR

Table S9 Expression real-time PCR primers (related to Figures 1, 3 and 7)

Gene	Forward Primer	Reverse primer
ActinB	CTAAGGCCAACCGTGAAAAG	ACCAGAGGCATAGGGACA
Dll1	GGGCTTCTCTGGCTTCAAC	TAAGAGTTGCCGAGGTCCAC
GAPDH	GGGTTCCTATAAATACGGACTGC	CCATTTTGTCTACGGGACGA
Hes1	TGAAGGATTCCAAAATAAAATTCTCTGGG	CGCCTCTTCTCCTGATAGGCTTTGATGAC
Hes5	AAGTACCGTGGCGGTGGAGAT	CGCTGGAAGTGGTAAAGCAGC
Id3	TCATAGACTACATCCTCGACCTTC	CACAAGTTCCGGAGTGAGC
Lfng	CCACTCCCACCTAGAGAACCT	ACTGCGTTCCGCTTGTTC
Lmcd1	GATCCATCCAAAGAAGTGGAA	TGTCAGCGTAGACCACAGG
MyT1	GGCCATGCATGAAAATGTACT	GCAATGGGACATCCAGATAAA
Notch1	CTGGACCCCATGGACATC	GGATGACTGCACACATTGC
Olig1	CAGGCCCAGTTCTCCAAG	GGGAAGATTGGCTGAGGTC
Sox2	AAGCGCCTTCATGGTATGGTC	TATAATCCGGGTGCTCCTTC
Tubb3	GCGCATCAGCGTATACTACAA	CATGGTTCCAGGTTCCAAGT

4. ChIP q-PCR

Table S10 ChIP-qPCR primers (related to Figures 1, 3 and 7)

Primers	Forward Primer	Reverse primer
Dll1 ORF (ORF1)	GTCTCAGGACCTTCACAGTAG	GAGCAACCTTCTCCGTAGTAG
Fbxw7 ORF (ORF2)	CTCGTCACATTGGAGAGTGG	CAGGAGCTTGGTTTCCTCAG
Hes1 ORF (ORF3)	CACTTTCTGCCTTCTGTGGA	AGAGGATGGAGGAGTCATGG
Hes1	GGGAAAGAAAGTTTGGGAAGT	GTTATCAGCACCAGCTCCAG
Hes5	GGGAAAAGGCAGCATATTGAGGCG	CACGCTAAATTGCCTGTGAATTGGCG
Id3	GAAAGGTTGCCTGGGACA	GTCTGCGCTGTTTTTGTTTC
Lfng	CTCCCCCACCACTAAGGAG	GGAGAGACACACAGGAAGCA
Lmcd1	ACAGGAAGGGCTGTTACCAT	CTGTTTGCTCTGTGTCTCTGG
MyT1	CTGGCAACACAATTCCAAAG	AGGGGTCATGCTGCTTCTAT
Notch1_1	ATTTGGCCAGAATTTGCATT	GCGCCACATTTAAACTCCTG
Notch1_2	CAGACCTGCTTAATTGGCTTC	GGAGACAGAGAAGGCTCCAG
Olig1	GTGAACAGTCCCCCTTCTGT	GCTGCCAAACCTTCAGTCTA
Sox2	CCGGAAACCCATTTATTCC	TGCAAACACTCTCTTCTCTGC

5. Cell culture

P19 and HEK293T cells were transfected by using linear polyethylenimine (PEI) (Sigma-Aldrich) in the proportion of DNA:PEI (w/w) of 1:2.5 for P19 cells and 1:3 for HEK293T cells. Total amount of DNA/cm^2, 500 ng. Medium was replaced with fresh medium 4-6h after transfection.

Mouse embryonic fibroblasts (MEFs) were isolated from E12.5 embryos. The head, vertebral column (containing the spinal cord), dorsal root ganglia and all internal organs were removed and discarded to ensure the removal of all cells with neurogenic potential from the cultures. The remaining tissue was manually dissociated and incubated 0.25% trypsin (Gibco) for 10-15 min to create a single cell suspension. The cells from each embryo were plated onto a T150 flask with MEF medium (Dulbecco's Modified Eagle Medium (DMEM) (BioWest) / High glucose containing 10% fetal bovine serum (FBS) (BioWest), 2mML-Glutamine (Gibco) and 100U/mL Penicillin/Streptomycin (Gibco)).

6. Antibodies

Table S11 Antibodies used in this study

Antigen (Species)	Working dilution IF: immunofluorescence WB: Western blot	Catalog number	Company / Reference
GFP (chicken)	1:1000 (IF)	06-896	Millipore
HA-tag (rabbit)	1:1000 (IF)	ab9110	Abcam
MyT1 (rabbit)	1:1000 (IF) ; 1:5000(WB)		Wang et al., 2007
MyT1L (guinea pig)	1:1000 (WB)		Tennant et al., 2012
MyT3 (rabbit)	1:2000 (WB)		Guogiang Gu et al.
Sox2 (rabbit)	1:500 (IF)	AB5603	Millipore
TubulinB III (mouse)	1:500 (IF)	MAB1637	Millipore
Alexa Fluor 488 Goat Anti-Chicken IgG	1:1000 (IF)		Life Technologies
Alexa Fluor 488 Goat Anti-mouse IgG	1:1000 (IF)		Life Technologies
Alexa Fluor 568 Goat Anti-rabbit IgG	1:1000 (IF)		Life Technologies
Alexa Fluor 568 Goat Anti-mouse IgG	1:1000 (IF)		Life Technologies
α-tubulin (mouse)	1:10 000 (WB)	T6074	Sigma
Goat Anti-Rabitt IgG (H+L) Poly-HRP	1:4000 (WB)		Jackson ImmunoResearch
Donkey Anti-Mouse IgG (H+L) Poly-HRP	1:4000 (WB)		Jackson ImmunoResearch

7. Image analysis and fluorescence quantification

All images were treated using ImageJ. The number of DAPI, Sox2-, MyT1-HA-positive cells was quantified using Threshold, Watershed and Analyze particles tools from ImageJ. The number of TuJ1-positive cells was quantified using the Cell Counter plugin from ImageJ. The number of cells counted per condition is mentioned in figures legends. Data is presented as mean ± SD.

8. Bioinformatics

Location analysis and expression data integration

MyT1 ChIP-Seq peak overlap with expression data from MyT1 GoF microarrays was calculated and plotted as heat maps with R/Bioconductor packages “genomeIntervals”, “gplots”, and in-house developed scripts.

Motif finding and Gene Ontology analysis

De novo search for differentially enriched motifs was performed using CisFinder (Sharov and Ko, 2009). Searches were run against a control dataset of identical length located 2Kb upstream (FDR<0.05%; Match threshold for clustering, 0.55). Motif fold enrichment (peaks/control) and percentage of peaks with motif were determined using the abundance tables obtained from CisFinder. Frequency distributions were plotted using the frequency tables obtained with CisFinder upon search within 2000bp regions centered on peak summits. Gene Ontology Biological Process analysis with functional annotation clustering was carried out using DAVID v6.7 (Dennis et al., 2003), using the whole microarray (MoGene 1.0 ST v1) as control (enrichment score (EASE)<0.05; similarity threshold for clustering, 0.8).

Density plots

ChIP-Seq normalized tag signals were calculated using a 10bp sliding window over the ± 2kb region around each peak summit to generate the occupancy profiles (in-house developed algorithm). These were plotted as heat maps of signal density using R/Bioconductor packages (http://www.Rproject.org/ and http://CRAN.R-project.org/package=gplots).

Gene expression analysis

NS5 Ascl1-ERT2 cells were plated in 6-well plates (600 000 cells/ well). Differentiation was induced 24h after plating by reducing EGF concentration to 5ng/mL and by adding 4-hydroxy-tamoxifen (TAM) (Sigma-Aldrich) (50nm). Samples were collected in triplicates 0, 4, 12, 24 and 48h post TAM.

Gene expression analysis using datasets from embryonic mouse telencephalon

Expression RNA-Seq data sets from single cells isolated from E11.5 mouse cortex are from (Hagey and Muhr, 2014). Analysis of the correlation of MyT1 and Hes1 expression was performed as previously described (Hagey and Muhr, 2014). Expression RNA-Seq data sets from cortical layers of the developing mouse brain at E14.5 are accessible at NCBI GEO database (Fietz et al., 2012), accession GSE38805. Hierarchical clustering of in vivo expression of genes bound and downregulated by MyT1 in culture was performed using distances based on the Pearson's correlation coefficient and plotted as a row-scaled heat map with R/Bioconductor “hclus” and “gplots” packages.

Hierarchical clustering of motif-containing ChIP-Seq peaks

Hierarchical clustering of ChIP-Seq peaks based on the presence or absence of the represented motifs. MyT1 motif and E-box were searched as consensus motifs. Rfx and Sox motifs were searched as positional weight matrices. Abundance tables obtained with the Cisfinder Search tool (Sharov and Ko, 2009) were converted to binary (1-presence, 0- absence). Only the peaks that have at least one of the motifs

searched are represented. Hierarchical clustering was plotted as heat maps with R/Bioconductor “hclust”, “heatmap” packages. P(MyT1 ChIP-Seq)>10^{-10}.

9. Publicly available data sets used in this study

Table S12 Data sets previously generated used in this study

Dataset	Reference
Ascl1-ERT2 ChIP-Seq in NS5 Ascl1-ERT2 cells, t=18h	Wapinski et al., 2013
H3K27ac ChIP-Seq in NS5 Ascl1-ERT2 cells, t=0h	Raposo et al., 2015
H3K4me1 in NS5 Ascl1-ERT2 cells, t=0h	Raposo et al., 2015
H3K4me3 ChIP-Seq in neural progenitor cells	Mikkelsen et al., 2007
H3K27me3 ChIP-Seq in neural progenitor cells	Mikkelsen et al., 2007
DNAse-Seq in proliferating and differentiating neural progenitor cells	Raposo et al., 2015

10. Supplemental references

Castro, D.S., Martynoga, B., Parras, C., Ramesh, V., Pacary, E., Johnston, C., Drechsel, D., Lebel-Potter, M., Garcia, L.G., Hunt, C., Dolle, D., Bithell, A., Ettwiller, L., Buckley, N., Guillemot, F., 2011. A novel function of the proneural factor Ascl1 in progenitor proliferation identified by genome-wide characterization of its targets. Genes Dev. 25, 930–45.

Dennis, G., Sherman, B.T., Hosack, D. a, Yang, J., Gao, W., Lane, H.C., Lempicki, R. a, 2003. DAVID: Database for Annotation, Visualization, and Integrated Discovery. Genome Biol. 4, P3.

Gohlke, J.M., Armant, O., Parham, F.M., Smith, M. V, Zimmer, C., Castro, D.S., Nguyen, L., Parker, J.S., Gradwohl, G., Portier, C.J., Guillemot, F., 2008. Characterization of the proneural gene regulatory network during mouse telencephalon development. BMC Biol. 6, 15.

Hagey, D.W., Muhr, J., 2014. Sox2 Acts in a Dose-Dependent Fashion to Regulate Proliferation of Cortical Progenitors. Cell Rep. 9, 1908–1920.

Raposo, A.A.S.F., Vasconcelos, F.F., Drechsel, D., Marie, C., Johnston, C., 2015. Ascl1 Coordinately Regulates Gene Expression and the Chromatin Landscape during Neurogenesis Article Ascl1 Coordinately Regulates Gene Expression and the Chromatin Landscape during Neurogenesis. Cell Rep. 1544–1556.

Sharov, A.L.A., Ko, M.I.S.H., 2009. Exhaustive Search for Over-represented DNA Sequence Motifs with CisFinder. DNA Res. 16, 261–273.

Yashiro-Ohtani, Y., He, Y., Ohtani, T., Jones, M.E., Shestova, O., Xu, L., Fang, T.C., Chiang, M.Y., Intlekofer, A.M., Blacklow, S.C., Zhuang, Y., Pear, W.S., 2009. Pre-TCR signaling inactivates Notch1 transcription by antagonizing E2A. Genes Dev. 23, 1665–1676.